OPEN ACCESS Freely available online

PLOS | COMPUTATIONAL BIOLOGY

An *In-Silico* Model of Lipoprotein Metabolism and Kinetics for the Evaluation of Targets and Biomarkers in the Reverse Cholesterol Transport Pathway

James Lu[1]*, Katrin Hübner[2], M. Nazeem Nanjee[3], Eliot A. Brinton[4], Norman A. Mazer[1]

1 F. Hoffmann-La Roche AG, pRED, Pharma Research & Early Development, Clinical Pharmacology, Basel, Switzerland, **2** BioQuant, University of Heidelberg, Heidelberg, Germany, **3** Division of Cardiovascular Genetics, University of Utah, Salt Lake City, Utah, United States of America, **4** Utah Foundation for Biomedical Research, Salt Lake City, Utah, United States of America

Abstract

High-density lipoprotein (HDL) is believed to play an important role in lowering cardiovascular disease (CVD) risk by mediating the process of reverse cholesterol transport (RCT). Via RCT, excess cholesterol from peripheral tissues is carried back to the liver and hence should lead to the reduction of atherosclerotic plaques. The recent failures of HDL-cholesterol (HDL-C) raising therapies have initiated a re-examination of the link between CVD risk and the rate of RCT, and have brought into question whether all target modulations that raise HDL-C would be atheroprotective. To help address these issues, a novel *in-silico* model has been built to incorporate modern concepts of HDL biology, including: the geometric structure of HDL linking the core radius with the number of ApoA-I molecules on it, and the regeneration of lipid-poor ApoA-I from spherical HDL due to remodeling processes. The ODE model has been calibrated using data from the literature and validated by simulating additional experiments not used in the calibration. Using a virtual population, we show that the model provides possible explanations for a number of well-known relationships in cholesterol metabolism, including the epidemiological relationship between HDL-C and CVD risk and the correlations between some HDL-related lipoprotein markers. In particular, the model has been used to explore two HDL-C raising target modulations, Cholesteryl Ester Transfer Protein (CETP) inhibition and ATP-binding cassette transporter member 1 (ABCA1) up-regulation. It predicts that while CETP inhibition would not result in an increased RCT rate, ABCA1 up-regulation should increase both HDL-C and RCT rate. Furthermore, the model predicts the two target modulations result in distinct changes in the lipoprotein measures. Finally, the model also allows for an evaluation of two candidate biomarkers for *in-vivo* whole-body ABCA1 activity: the absolute concentration and the % lipid-poor ApoA-I. These findings illustrate the potential utility of the model in drug development.

Citation: Lu J, Hübner K, Nanjee MN, Brinton EA, Mazer NA (2014) An *In-Silico* Model of Lipoprotein Metabolism and Kinetics for the Evaluation of Targets and Biomarkers in the Reverse Cholesterol Transport Pathway. PLoS Comput Biol 10(3): e1003509. doi:10.1371/journal.pcbi.1003509

Editor: Daniel A. Beard, University of Michigan, United States of America

Received September 2, 2013; **Accepted** January 22, 2014; **Published** March 13, 2014

Funding: This work was supported by the Roche Postdoctoral Fellowship fund of F. Hoffmann-La Roche AG, Basel, Switzerland, project number RPF-153. The funders had no role in study design, data collection and analysis, decision to publish, or preparation of the manuscript.

Competing Interests: I have read the journal's policy and have the following conflicts: JL and NAM are employees of F. Hoffmann-La Roche; JL and NAM have stock ownership of F. Hoffmann-La Roche. KH, MNN and EAB declare no competing interest.

* E-mail: james.lu.jl1@roche.com

Introduction

Epidemiological studies have shown that high levels of low-density lipoprotein cholesterol (LDL-C) as well as low levels of high-density lipoprotein cholesterol (HDL-C) are associated with increased cardiovascular disease (CVD) risk [1,2]. While LDL-C lowering therapies have been shown consistently to reduce CVD risk, there is significant residual risk that remains to be managed [2]. The strong inverse association between HDL-C and CVD risk has led to the "HDL-C hypothesis", whereby all HDL-C raising therapies should be anti-atherogenic [2,3]. Currently, the anti-atherogenic activity of HDL is mainly attributed to its role in mediating reverse cholesterol transport (RCT), whereby cholesterol is effluxed from peripheral tissues and transported to the liver for biliary excretion [4]. However, the recent failures of a number of HDL-C raising intervention trials [5–7] have called for a re-examination of the HDL-C hypothesis. It has long been thought that HDL-C is a reliable biomarker for cholesterol efflux from tissues [8]. However, the several recent failed HDL-C raising intervention trials provide mounting evidence that at least under certain conditions, the plasma concentration of HDL-C, a very simple and static measure, is inadequate for characterizing the rate of RCT, which is a complex and dynamic process [8]. A revision of the HDL-C hypothesis to the "HDL flux hypothesis" has been proposed, whereby interventions should be aimed at promoting cholesterol efflux to HDL, and hence the overall RCT rate, independently of their effects on HDL-C levels [9,10]. Hence, there is now a pressing need to better understand the role of HDL-C raising targets in the context of RCT and to identify biomarkers which could provide information on the flux rate through the RCT pathway [8]. Our modeling effort is focused on addressing these issues.

A number of previous mathematical models have focused on various aspects of lipid metabolism; see [11,12] for recent reviews. Of the existing models, some describe metabolic processes at a mechanistic level [13–19], while others have been empirically derived from tracer kinetic studies [20–22]. In general these models were built to describe the dynamics of HDL and the other

Author Summary

Epidemiological studies have shown a strong inverse association between HDL-C and cardiovascular risk and led to the formulation of the "HDL cholesterol hypothesis": under this hypothesis, interventions raising HDL-C should decrease risk. However, the recent failures of HDL-C raising therapies in improving cardiovascular disease risk in outcomes trials have suggested a need to revise the hypothesis to account for the contrary data. An "HDL flux hypothesis" has emerged: it is not HDL-C level *per se* which forms the basis for reducing risk, but it is the flux rate of reverse cholesterol transport that drives risk reduction. We propose that, the concentration of HDL cholesteryl ester in plasma simply reflects the ratio of input rate of reverse cholesterol transport into the HDL compartments to its clearance rate. A challenge in identifying targets under the new conceptual framework is the feedback process that occurs between the input rate and the clearance rate of HDL-C. To meet this challenge, we have built a systems model which incorporates the main processes of HDL metabolism to elucidate the relationships between target modulations and the reverse cholesterol transport rate.

major lipoprotein classes, which include LDL, intermediate density lipoprotein (IDL) and very low density lipoprotein (VLDL), describing lipid transport between these particles mediated by the cholesteryl ester transport protein (CETP) in the normal or basal state, and the effects of genetic mutations and/or drug interventions on these processes. While valuable insights have been gained from these models, none can be used to predict the associated changes in the RCT rate since they lack a mechanistic description of ApoA-I dynamics and other key processes involved in the RCT pathway. The latter include the lipidation of lipid-poor ApoA-I via its interaction with ATP-binding cassette transporter member 1 (ABCA1), the key process in the initiation of RCT [8], as well as processes of HDL remodeling which lead to the delivery of cholesterol from HDL to other lipoproteins and cells, and the regeneration of lipid poor ApoA-I [23]. In all the existing models except the ones by Hübner *et al* [16] and Adiels *et al* [24], the dynamics of apolipoproteins that cover the surface of lipoprotein particles are not described. While each VLDL, IDL and LDL particle contains only one ApoB molecule per particle, for HDL particles the number of ApoA-I molecules per particle may vary from 2 to 4 or more depending on HDL size [25]. This variation results from HDL remodeling processes such as particle fusion, CETP-mediated lipid transport, lipolysis and esterification whereby particles can gain or lose core lipid content as well as ApoA-I molecules [23]. While it has been shown experimentally and theoretically that the number of ApoA-I molecules on a given HDL particle is intrinsically linked to the particle size [25], this important relationship has yet to be incorporated into a mechanistic model of HDL metabolism.

In this paper, we propose a novel model of lipoprotein metabolism and kinetics (the LMK model) that provides an integrated description of the dynamics of cholesterol and ApoA-I in plasma. In particular, the model captures the initiation of RCT from the lipidation of lipid-poor ApoA-I by the ABCA1 transporter, the generation of nascent discoidal and nascent spherical particles, HDL particle fusion, CETP mediated lipid transfer between HDL and other lipoproteins, and the dissociation of excess ApoA-I from mature spherical α-HDL due to remodeling processes. The model is calibrated to: lipoprotein measures for normal and CETP deficient subjects; cholesteryl ester (CE) and ApoA-I fluxes measured in normal subjects; data on the fractional catabolic rate (FCR) of ApoA-I. The structure and the kinetic constants of our model provide an explanation for the relationship between FCR of ApoA-I and HDL particle size. To our knowledge the LMK model is the first to provide a mechanistic basis for the linkage between the metabolism of ApoA-I and the cholesterol component of HDL. The model has been validated by simulating patients with genetic mutations in the HDL metabolism pathway and the predictions are compared with lipoprotein measures reported in literature. Finally, the model was used to evaluate targets that could potentially increase RCT and to identify relevant biomarkers, as part of the effort to support drug discovery and development using a model-based approach.

Results/Discussion

Model structure

The LMK model is shown schematically in Figure 1, focused on the RCT pathway and a number of targets contained within it, for instance CETP, ABCA1, ApoA-I and SRB1. The LMK model describes the synthesis of ApoA-I and the initiation of RCT by the interaction of lipid-poor ApoA-I with ABCA1 leading to the formation of mature, spherical α-HDL. The HDL remodeling processes represented in the model include: the fusion of spherical HDL particles (arrow 5 of Figure 1); the exchange and elimination of CE in spherical HDL by interaction with CETP (arrows 12–14) and SRB1 (arrow 7); the regeneration of lipid-poor ApoA-I from spherical HDL particles (arrow 3). Lipid-poor ApoA-I is assumed to be eliminated via the kidney (arrow 4), while the spherical HDL particles are assumed to be eliminated by a holo-uptake mechanism with a rate dependent on the particle size (arrow 6). The transfer and elimination of CE in LDL and VLDL pools are also represented (arrows 9–11). Our approach is to adequately describe the metabolic processes, while keeping the model as simple as possible. The representations of lipoprotein components and metabolic processes in the LMK model reflect these principles.

Lipoprotein representation. While HDL particles are heterogeneous in size and composition [8], for the purposes of understanding RCT we only consider two HDL particle classes: spherical, α-HDL and small, lipid-poor ApoA-I. Amongst the apolipoproteins and lipid species contained in α-HDL particles, the LMK model has an explicit representation of ApoA-I and CE. Although there are a large number of species in the HDL proteome (e.g., ApoA-II, ApoE) and lipidome (e.g., triglycerides, phospholipids) which may be relevant in particular diseased states, they play a secondary role in the characterization of RCT. We make the assumption that the protein moiety contains 60% ApoA-I by weight, with all other proteins contributing the remaining 40%. This is within the range of values reported in literature [25,26]. Under this assumption, the total concentration of ApoA-I is represented as an explicit variable that changes as a direct result of the metabolic processes described in the model while ApoA-II and other HDL apolipoproteins are implicit quantities: namely, they are assumed to change in concert with ApoA-I so as to keep the weight fraction constant. Similarly, the LMK model explicitly represents CE in the particle classes of α-HDL, VLDL and LDL but represents TG in α-HDL only implicitly. That is, the ratio of TG/CE in α-HDL particles is assumed to be 13% which is consistent with the range of values reported in healthy subjects [25,27]. The amounts of free cholesterol (FC) and phospholipids (PL) per HDL particle are implicitly represented in the LMK model: they depend on the α-HDL size, in a manner analogous to the treatment of PL in [16]. In particular, given the CE content of

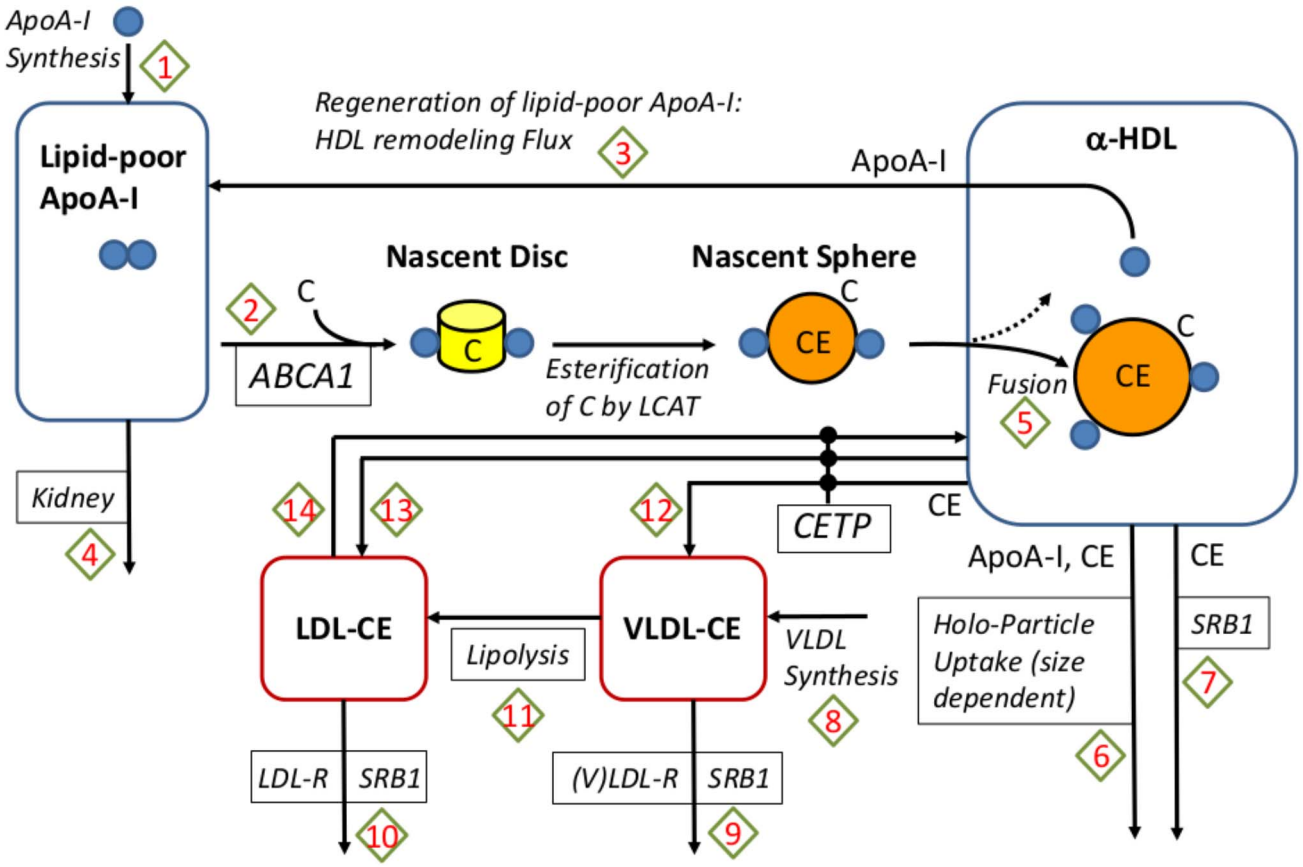

Figure 1. A schematic representation of the model. The arrows shown in the diagram denote the processes represented by the model and the boxes with italicized text denote mediators that are explicitly represented. The process arrows are numbered, refering to the reaction number shown in Table 2. The arrows leading from the nascent sphere towards the α-HDL pool represent the 2 scenarios that may occur in the transformation of newly formed particles: they may either enter the α-HDL pool as distinct particles (the dashed arrow) or fuse with the existing ones (solid arrow).
doi:10.1371/journal.pcbi.1003509.g001

an α-HDL particle its core size can be inferred and the FC and PL content on the surface can be computed using the updated Shen model; see [25]. With our choice of lipoprotein representation, the species represented in the model are given in Table 1.

Metabolic processes. The full list of reactions represented in the LMK model (as schematized in Figure 1) is shown in Table 2. We would like to point out that the remodeling flux (arrow 3 of Figure 1) based on geometric concepts developed in [25] is an original contribution of our work. The remodeling flux expression, $F_{\mathrm{rem}}(\mathrm{CE}_\alpha(t),A_\alpha(t),N_\alpha(t))$, represents the excess ApoA-I within the pool of α-HDL particles given the core cholesteryl ester content, particle concentration and the amount of ApoA-I covering the surface. Its derivation based on geometric concepts of α-HDL particles is discussed in more detail in the Methods section. The holo-uptake of α-HDL particles is thought to be mediated by a number of receptors, which are not well understood [28,29]. In order to account for the possible size-dependence in the uptake rate of α-HDL particles, the functional dependence $k_{\mathrm{holo}}(d)$ is utilized. This is also discussed in more detail in the Methods section.

Table 1. Species represented in the model.

Symbol	Description	Units
A_{lp}	Lipid-poor ApoA-I	mg/dL
A_α	ApoA-I in the α-HDL pool	mg/dL
N_α	Particle concentration of α-HDL	mmol/dL
CE_α	cholesteryl ester in α-HDL	mg/dL
$\mathrm{CE}_{\mathrm{LDL}}$	cholesteryl ester in LDL	mg/dL
$\mathrm{CE}_{\mathrm{VLDL}}$	cholesteryl ester in VLDL	mg/dL

doi:10.1371/journal.pcbi.1003509.t001

The model constants are shown in Table 3 while the list of parameters are given in Table 4; the prior values of parameters and their posterior estimates are discussed in the next section. With the list of reactions given in Table 2, the LMK model can be expressed as the following system of ODEs:

$$\frac{dA_{lp}(t)}{dt} = r_{\mathrm{in}}^{lp} - k_{\mathrm{ABCA1}}A_{lp}(t) - k_{\mathrm{kidney}}A_{lp}(t) + k_{\mathrm{dissoc}}F_{\mathrm{rem}}(\mathrm{CE}_\alpha(t),A_\alpha(t),N_\alpha(t)) \quad (1a)$$

$$\frac{dA_\alpha(t)}{dt} = k_{\mathrm{ABCA1}}A_{lp}(t) - k_{\mathrm{dissoc}}F_{\mathrm{rem}}(\mathrm{CE}_\alpha(t),A_\alpha(t),N_\alpha(t)) - k_{\mathrm{holo}}(d)A_\alpha(t) \quad (1b)$$

Table 2. Reactions represented in the model.

#	Reaction	Description	Rate expression	Ref.
1	$\varnothing \rightarrow A_{lp}$	ApoA-I synthesis	r_{in}^{lp}	[22,88]
2	$A_{lp} \rightarrow A_\alpha + \gamma \frac{m_C}{m_A}\text{CE}_\alpha + \frac{N_\alpha}{2m_A}$	Initiation of RCT by interaction with ABCA1	$k_{\text{ABCA1}} A_{lp}(t)$	[79,80,89]
3	$A_\alpha \rightarrow A_{lp}$	Regeneration of lipid-poor ApoA-I via HDL remodeling	$k_{\text{dissoc}} \times F\text{rem}(\text{CE}_\alpha(t), A_\alpha(t), N_\alpha(t))$	[22,25,76,90–92]
4	$A_{lp} \rightarrow \varnothing$	Kidney removal of lipid-poor ApoA-I	$k_{\text{kidney}} A_{lp}(t)$	[43,48]
5	$N_\alpha \rightarrow \varnothing$	Fusion of nascent spherical particles with mature α-HDL	$\frac{k_{\text{ABCA1}} A_{lp}(t)}{2m_A} \frac{k_f N_\alpha(t)}{1+k_f N_\alpha(t)}$	[23,93]
6	$\{A_\alpha, \text{CE}_\alpha, N_\alpha\} \rightarrow \varnothing$	HDL particle holo-uptake	$k_{\text{holo}}(d) \times \{A_\alpha(t), \text{CE}_\alpha(t), N_\alpha(t)\}$	[28,29]
7	$\text{CE}_\alpha \rightarrow \varnothing$	SR-B1 mediated removal of CE from HDL particles	$k_{\text{SRB1}}^{\text{HDL}} \text{CE}_\alpha(t)$	[4,8,18,36]
8	$\varnothing \rightarrow \text{CE}_{\text{VLDL}}$	Synthesis of CE in VLDL	$r_{\text{in}}^{\text{VLDL}}$	[20,21]
9	$\text{CE}_{\text{VLDL}} \rightarrow \varnothing$	Elimination of CE from VLDL	$k_{\text{out}}^{\text{VLDL}} \text{CE}_{\text{VLDL}}(t)$	[20,21]
10	$\text{CE}_{\text{LDL}} \rightarrow \varnothing$	Elimination CE from LDL	$k_{\text{out}}^{\text{LDL}} \text{CE}_{\text{LDL}}(t)$	[20,21]
11	$\text{CE}_{\text{VLDL}} \rightarrow \text{CE}_{\text{LDL}}$	VLDL conversion to LDL via lipolysis	$k_{\text{VL}} \text{CE}_{\text{VLDL}}(t)$	[20]
12	$\text{CE}_\alpha \rightarrow \text{CE}_{\text{VLDL}}$	CETP mediated CE transfer from HDL to VLDL	$k_{\text{HV}}^{\text{CETP}} \text{CE}_\alpha(t)$	[13,17,18,20,30]
13	$\text{CE}_\alpha \rightarrow \text{CE}_{\text{LDL}}$	CETP mediated CE transfer from HDL to LDL	$k_{\text{HL}}^{\text{CETP}} \text{CE}_\alpha(t)$	[13,20,30]
14	$\text{CE}_{\text{LDL}} \rightarrow \text{CE}_\alpha$	CETP mediated CE transfer from LDL to HDL	$k_{\text{LH}}^{\text{CETP}} \text{CE}_{\text{LDL}}(t)$	[13,18,20,30]

doi:10.1371/journal.pcbi.1003509.t002

$$\frac{dN_\alpha(t)}{dt} = \frac{k_{\text{ABCA1}}}{2m_A}\frac{1}{1+k_f N_\alpha(t)} A_{lp}(t) - k_{\text{holo}}(d) N_\alpha(t) \quad (1c)$$

$$\frac{d\text{CE}_\alpha(t)}{dt} = \gamma \frac{m_C}{m_A} k_{\text{ABCA1}} A_{lp}(t) + k_{\text{LH}}^{\text{CETP}} \text{CE}_{\text{LDL}}(t) - \left[k_{\text{HV}}^{\text{CETP}} + k_{\text{HL}}^{\text{CETP}} + k_{\text{SRB1}}^{\text{HDL}} + k_{\text{holo}}(d)\right] \text{CE}_\alpha(t) \quad (1d)$$

$$\frac{d\text{CE}_{\text{LDL}}(t)}{dt} = k_{\text{VL}} \text{CE}_{\text{VLDL}}(t) + k_{\text{HL}}^{\text{CETP}} \text{CE}_\alpha(t) - (k_{\text{LH}}^{\text{CETP}} + k_{\text{out}}^{\text{LDL}}) \text{CE}_{\text{LDL}}(t) \quad (1e)$$

$$\frac{d\text{CE}_{\text{VLDL}}(t)}{dt} = r_{\text{in}}^{\text{VLDL}} + k_{\text{HV}}^{\text{CETP}} \text{CE}_\alpha(t) - (k_{\text{VL}} + k_{\text{out}}^{\text{VLDL}}) \text{CE}_{\text{VLDL}}(t). \quad (1f)$$

One important quantity that the LMK model can help to assess is the rate of *reverse cholesterol transport* (RCT) at the whole-body level. This quantity is thought to play an important role in determining cardiovascular disease risk, but is experimentally challenging to assess. Using the LMK model, we are able to quantify the flux rate of free cholesterol into the nascent disc particles mediated by ABCA1: in particular, this is given by

$$\text{RCT rate} = \text{plasma volume} \times \gamma \frac{m_C}{m_A} k_{\text{ABCA1}} A_{lp}(t). \quad (2)$$

The term $k_{\text{ABCA1}} A_{lp}(t)$ represents the transformation rate of lipid-poor ApoA-I to nascent discs, which subsequently enter the α-HDL pool. The parameter γ describes the number of cholesterol molecules per ApoA-I in the nascent discs. $\frac{m_C}{m_A}$ converts the molecular mass of ApoA-I to cholesterol. Finally, the volume of plasma converts RCT rate to the whole-body level: we assume that plasma volume = 3.15 L in a 70 kg adult [22]. As illustrated in Figure 1, nascent discs are transformed into nascent spheres (as mediated by the LCAT enzyme [30]) which are assumed to have in their cores γ CE molecules per ApoA-I. Hence, the RCT expression (2) also represents the input rate of HDL-CE into the plasma α-HDL pool. Note that the factor 2 in the expression for reaction 2 (initiation of RCT) accounts for the assumption that there are 2 ApoA-I molecules per nascent HDL particle.

Model calibration

Parameter estimates: Prior and posterior. The Bayesian approach for parameter estimation is a well established methodology which has found applications in various fields of science [31], including parameter estimation for models of cellular processes [32,33] as well as pharmacokinetics and pharmacodynamics (PK/PD) [34,35]. Under this framework, it is assumed that a prior distribution is available for (some) parameters as a result of previous experimental studies. In combination with calibration data, the posterior distribution for the parameters is obtained.

For most of the LMK model parameters, prior estimates are available from literature studies; a detailed discussion of the references from which parameter estimates and their uncertainties are obtained is given in the Methods section. Using the model calibration procedure as discussed in the Methods section, the prior is combined with calibration data to give rise to the posterior estimates. A list of the prior and posterior values of parameters is given in Table 5. It is worthwhile noting that, for the most part, the *maximum a posteriori* (MAP) estimate obtained by the calibration process does not depart significantly from the prior. This indicates that the calibration data are fairly consistent with the prior

estimates. One exception is the parameter $k_{\mathrm{SRB1}}^{\mathrm{HDL}}$, which is increased significantly from its prior beyond the 1 SD value. This result is in agreement with experimental evidence that SRB1 plays a significant role in mediating HDL-CE removal from HDL particles [36], in contrast to the expectation of a previous tracer kinetics study [21]. The discrepancy may be attributed to the limitation of tracer kinetics studies (for instance, [21]) to be able to fully identify the SRB1 contribution. Finally, it can be seen that the calibration data are sufficiently informative to allow relatively precise estimates for the parameters k_{holo}^{l} and k_f, for which there was no prior information. It is worth noting the negative sign in the estimate for k_{holo}^{l}, which implies that the α-HDL holo-particle uptake rate decreases with particle size. The sign of this size-dependence is consistent with the hepatic endocytic receptor (mitochondrial ATP synthase subunit β) having a higher affinity for the (smaller) HDL-3 as compared to the (larger) HDL-2 [29,37,38].

Calibration data and model explanatory power. In order to identify parameter values using the Bayesian approach, calibration data are needed. However, the choice of calibration data should be made not only for the purpose of quantifying parameters, but also with the consideration for the potential utility and the explanatory power of the model. More specifically, choosing the right types of calibration data can help to increase confidence in a model's predictions of specific scenarios; in addition, model calibration is also an opportunity to test if the model structure, together with prior information on the parameter values, can explain important features of the system being studied.

In our current work, the LMK model was used to explain the effects of CETP inhibition on ApoA-I level as well as the inverse relationship between the FCR of ApoA-I and particle size. Based on this, the calibration data were chosen. In Figures 2, 3 and 4 we show the calibration data superimposed with the model simulation, using the *maximum a posteriori* parameter set identified by the calibration procedure (as described in the Methods section). In Figure 2, the decrease in CETP level from 100% to 0% of the nominal subject was simulated by decreasing the three parameters associated with CETP activity ($k_{\mathrm{HV}}^{\mathrm{CETP}}, k_{\mathrm{HL}}^{\mathrm{CETP}}, k_{\mathrm{LH}}^{\mathrm{CETP}}$) by the same factor. In particular, panels A and B show that the rise in HDL-C (the concentration of HDL-C is computed by summing CE_{α} and free cholesterol pool, as discussed in the Methods section) and ApoA-I in heterozygotes and homozygotes with CETP deficiency are fairly well captured by the LMK model; the main discrepancy is the under-prediction of HDL-C for CETP heterozygotes. To our knowledge, the increase in ApoA-I under CETP deficiency or inhibition has not yet been explained by existing models: by incorporating the geometric ideas proposed in [25] the LMK model provides, for the first time, a way to connect the metabolism of ApoA-I and HDL-C. We remark that the LMK model is focused on HDL rather than the metabolism of ApoB-containing particles, which include LDL and VLDL. In particular, the LMK model predicts negligible concentrations of LDL-CE and VLDL-CE in CETP homozygotes, which are inconsistent with the reported concentrations in these subjects [39–41]. We believe that this discrepancy between the LMK model prediction and reality is due to β-LCAT activity [42], which in CETP homozygotes could compensate for the lack of CE influx from HDL particles by converting free cholesterol on the surface of ApoB-containing particles into cholesteryl ester. Finally, Figure 3 shows that the CE fluxes in the LMK model are consistent with the values measured [20], in particular the CE flux from HDL to LDL is close to that from LDL to HDL.

Another important and robust finding that has been observed in HDL metabolism is the relationship between FCR of ApoA-I and particle size (estimated using a surrogate measure) seen in normal subjects [43,44]; in addition, heterozygotes and homozygotes of CETP deficiency are also observed to have a decreased FCR of ApoA-I [45]. Thus, an important objective of the calibration process is to test whether the structure of the model, together with an assumption on the linear size-dependence of HDL holo-particle uptake rate, can explain this relationship. The inverse relationship observed between the FCR of ApoA-I and the ratio HDL-C/ApoA-I (a surrogate measure of HDL size) is shown in Figure 4: in particular, data from Schaefer *et al* [44], Brinton *et al* [43] and Ikewaki *et al* [45] are given. A linear fit was carried out using the pooled data of Schaefer *et al* [44], Brinton *et al* [43] and normal subjects from Ikewaki *et al* [45], with the mean shown as a dashed pink line and the 1 SD confidence region shown as dashed black lines in Figure 4. The ApoA-I FCR for CETP homozygotes (who have large HDL particles) are assumed to be the lowest level attainable, hence this value was taken as the "floor" of the fit. The LMK model was calibrated to the piecewise linear relationship represented by the pink line and Figure 4 shows that simulations for normal and CETP mutation subjects (denoted by the asterisk symbols) are all in good agreement with the inverse relationship. The LMK model reproduces the dependence of ApoA-I FCR on CETP primarily by changing the distribution of ApoA-I between the lipid-poor and α-HDL pools (which have different clearance rates), with a minor contribution from the explicit size dependence of holo-particle uptake, $k_{\mathrm{holo}}(d)$.

Table 3. Model constants.

Constant	Description	Unit	Value	Ref.
m_A	Molecular weight of ApoA-I	g/mol	28500	[16]
m_C	Molecular weight of cholesterol (free and esterified)	g/mol	386	[16]
V_{CE}	Molecular volume of cholesteryl ester	Å^3	1068	[25]
V_{TG}	Molecular volume of triglyceride	Å^3	1556	[25]
t	Thickness of HDL surface	Å	20.2	[25]

By convention, the cholesteryl ester mass is measured by quantifying the equivalent mass of free cholesterol.
doi:10.1371/journal.pcbi.1003509.t003

Model validation

In order to increase confidence in its predictions, the LMK model has been validated by simulating a number of scenarios that have not been used in the calibration process. In particular, since ABCA1 and ApoA-I are important targets in the pathway, the literature data on subjects with mutations in these genes [46,47] are compared against the model simulations. The heterozygotes and homozygotes of ABCA1 mutation are simulated by setting k_{ABCA1} (representing ABCA1 activity) to 50% and 0% of its nominal value respectively; similarly, heterozygotes and homozygotes of ApoA-I mutation are simulated by setting the parameter r_{in}^{lp} (representing ApoA-I synthesis rate) to 50% and 0% of its nominal value respectively. Figure 5 shows the mean and 95% confidence intervals of the model simulations, compared to the literature data (mean and SD are given). An examination of the results for the heterozygotes shows that, encouragingly, the LMK model is able to differentiate between the effects of ABCA1 and ApoA-I mutations on HDL-C and ApoA-I levels: both quantities

Table 4. Model parameters.

	Description	Unit
r_{in}^{lp}	Synthesis rate of ApoA-I	mg/dL/day
k_{kidney}	Rate of kidney elimination	pool/day
k_{dissoc}	Dissociation rate of excess ApoA-I	pool/day
k_{ABCA1}	Rate constant in the lipidation of lipid-poor ApoA-I via ABCA1	pool/day
γ	Stoichiometry of FC to ApoA-I in nascent discs	unitless
$k_{\text{HV}}^{\text{CETP}}$	Rate constant of CE transfer: HDL to VLDL	pool/day
$k_{\text{HL}}^{\text{CETP}}$	Rate constant of CE transfer: HDL to LDL	pool/day
$k_{\text{LH}}^{\text{CETP}}$	Rate constant of CE transfer: LDL to HDL	pool/day
k_{VL}	Rate constant of CE transfer: VLDL to LDL	pool/day
$r_{\text{in}}^{\text{VLDL}}$	Synthesis rate of CE to VLDL	mg/dL/day
$k_{\text{out}}^{\text{VLDL}}$	Rate constant of CE elimination from VLDL	pool/day
$k_{\text{out}}^{\text{LDL}}$	Rate constant of CE elimination from LDL	pool/day
$k_{\text{SRB1}}^{\text{HDL}}$	Rate constant of SRB1-mediated CE elimination from HDL	pool/day
k_{holo}^{c}	Constant contribution to the rate of α-HDL holo-particle uptake	pool/day
k_{holo}^{l}	Size-dependent contribution to the rate of α-HDL holo-particle uptake	pool/day/nm
k_f	Parameter governing the particle concentration dependence of fusion rate	1/(mmol/dL)

doi:10.1371/journal.pcbi.1003509.t004

decrease more for ApoA-I heterozygotes as compared to ABCA1 heterozygotes. Furthermore, the LMK model predicts that heterozygotes of ABCA1 mutation have smaller HDL particles (data not shown), consistent with the data of Asztalos *et al* [46].

Most of the calibration data are static in nature, hence it is of particular interest to perform dynamic simulations of the LMK model and compare them to existing data. As a validation, we would like to see if the LMK model reproduces the characteristic biphasic decay curves seen in tracer kinetic experiments with labelled ApoA-I. In the LMK model, the injection of radio-labelled dose is represented by a small addition to the pool of lipid-poor ApoA-I and the fractional dose remaining in the sum of the two pools of ApoA-I is plotted; refer to the Methods section for the details of the simulation methodology. This is simulated using the parameters identified for the nominal subject and the result is shown in Figure 6: it can be seen that the simulated decay curve is biphasic and similar to the data obtained by digitizing Figure 3 of Ikewaki *et al* [48]. Furthermore, the mean residence time (which is the inverse of FCR) of labelled ApoA-I computed from the model simulation is 4.2 days, which is in good agreement with the result of 4.8 ± 0.3 days as measured in 4 subjects by Ikewaki *et al* [48].

Explaining epidemiological relationship using a virtual population

Having calibrated and validated the LMK model, we use it as a platform for exploring the observed epidemiological relationship between HDL-C and CVD risk. For this purpose, a virtual population is generated in a manner analogous to that of reference [49]. In particular, model parameters are sampled from a multivariate normal distribution and for each set of parameters the "phenotype" of the corresponding virtual subject is simulated using the LMK model. As there is no information available on the correlation between model parameters in a real population, we have assumed them to be uncorrelated and each is drawn from a normal distribution with a relative SD = 15% around the value corresponding to the posterior values for the nominal subject (see Table 5).

Despite the fact that the parameter distribution in the virtual population is uncorrelated, some of the simulation outputs show significant correlations as a result of the model structure. Of particular interest is the correlation between RCT rate (as defined in (2)) and plasma biomarkers. Shown in Figure 7 is the relationship between RCT rate and HDL-C within the virtual population: it can be seen that there is a surprisingly strong correlation between the two quantities ($r = 0.95$). We note that the RCT rate given in (2) corresponds to the input rate of HDL-CE into plasma: in fact, the plasma concentration of HDL-CE can be expressed as the following:

$$\text{HDL}-\text{CE} = \frac{\text{RCT rate}}{\text{Clearance rate of HDL}-\text{CE}} \qquad (3)$$

where the clearance is defined as the plasma volume multiplied by the sum of elimination rate constants. In the LMK model, elimination processes for HDL-CE include those mediated by CETP and SRB1, as well as the holo-particle uptake. While the RCT rate shows a strong correlation with HDL-C, we see that in Figure 8 the clearance of HDL-CE shows a much weaker negative correlation with HDL-C ($r = -0.32$). Hence, the simulation results suggest that the variation in HDL-C within the virtual population is largely attributed to variations in the RCT rate and not due to its clearance. Under the "HDL flux hypothesis" [2] that low RCT rate results in high CVD risk, the relationship shown in Figure 7 provides a plausible explanation for the epidemiological association between HDL-C and CVD risk. The same set of virtual subjects is also used in subsequent sections for target evaluation and biomarker identification.

Table 5. Prior and posterior estimates of model parameters corresponding to the "nominal subject."

Parameter	Prior (mean±SD)	Posterior (mean±SD)
r_{in}^{lp}	27.44±1.18	28.46±1.13
k_{kidney}	5.19±2.60	2.42±0.78
k_{dissoc}	174±312	170±191
k_{ABCA1}	96.24±17.55	95.18±15.73
γ	7.55±3.94	10.17±2.19
$k_{\text{HV}}^{\text{CETP}}$	1.47±0.58	1.49±0.24
$k_{\text{HL}}^{\text{CETP}}$	5.47±2.05	6.92±0.81
$k_{\text{LH}}^{\text{CETP}}$	1.98±0.70	2.89±0.34
k_{VL}	7.52±0.94	7.70±0.84
$r_{\text{in}}^{\text{VLDL}}$	0.96±0.46	1.50±0.45
$k_{\text{out}}^{\text{VLDL}}$	0.88±0.37	1.30±0.35
$k_{\text{out}}^{\text{LDL}}$	0.67±0.08	0.64±0.07
$k_{\text{SRB1}}^{\text{HDL}}$	0.31±0.12	0.60±0.08
k_{holo}^{c}	0.14±0.026	0.13±0.022
k_{holo}^{l}	0	−0.016±0.004
k_f	0	5000±1544

The prior parameter values were estimated from literature as discussed under the Methods section. The SDs of the posterior distribution were estimated using the Fisher Information Matrix.

doi:10.1371/journal.pcbi.1003509.t005

HDL-C raising therapies

The LMK model can be used to evaluate actual and potential HDL-C raising therapies, by modulating targets of interest. We have used simulated the model for both the nominal subject, as well as for a virtual population.

CETP inhibition. The model predictions of CETP inhibition on the nominal subject, together with 95% confidence intervals, are shown in Figure 9. In alignment with the calibration data, as CETP level decreases both HDL-C and ApoA-I increase strikingly (see panels A and B). These changes are associated with a significant increase in HDL size as well as a small increase in HDL particle concentration (HDL-P) (see panels C and D). Both the absolute concentration of lipid-poor ApoA-I and RCT rate remain essentially unchanged (see panels E and F).

To further illustrate the effect of CETP inhibition, in Figure 10 we simulate the therapy in a virtual population. In particular, we select subjects with low HDL-C (40 mg/dL or less) for treatment with a hypothetical drug that inhibits the plasma CETP by 80% and simulate the changes in HDL-C and RCT rate in the treated subjects. It can be seen that the rise in HDL-C does not correspond to an increase in RCT rate. In fact, the effects induced by CETP inhibition depart from the baseline relationship. This is an illustration of a target impacting a biomarker which is correlated but not causally linked with the disease mechanism: the hypothetical drug does not bring about a therapeutic effect of increasing RCT rate despite increasing HDL-C. However, there could be a potential CV benefit due to a small (14%) decrease in LDL-C (data not shown).

ABCA1 up-regulation. The model predictions for ABCA1 up-regulation on the nominal subject, together with 95% confidence intervals, are shown in Figure 11. The simulation results show that as ABCA1 activity increases, both HDL-C and ApoA-I increases (see panels A and B). Panels C and D of Figure 11 show that these increases reflect not only an increase in HDL size, but also increases in particle concentration. In stark contrast to CETP inhibition, under ABCA1 upregulation the RCT rate is predicted to increase markedly (panel E) and the absolute concentration of lipid-poor ApoA-I decreases.

We next consider ABCA1 up-regulation for the virtual population as shown in Figure 7. In particular, we select the same subjects with low HDL-C as was previously chosen for CETP inhibition. We simulate a hypothetical drug that increases ABCA1 activity in each of the treated subjects by 100% and examine the changes in HDL-C and RCT rate. As shown in Figure 12, under ABCA1 up-regulation both HDL-C and RCT rate increase. In particular, the changes induced by ABCA1 up-regulation are predicted to follow the baseline epidemiological relationship.

In order to further elaborate on the differences between the two target modulations, we compare in Figure 13 the changes in biomarkers for CETP inhibition and ABCA1 up-regulation. The simulation results show that for a given fold change in HDL-C, CETP inhibition gives rise to larger particle sizes but fewer particle numbers as compared to ABCA1 up-regulation. Due to the differences in the particle size and number under the two target modulations, for a given fold-change in HDL-C, ApoA-I is predicted to increase more under ABCA1 up-regulation as compared to CETP inhibition. Reassuringly, the simulated increases in ApoA-I for CETP inhibition are in fair agreement with literature data for the three CETP inhibitors, Dalcetrapib [50], Torcetrapib [51] and Anacetrapib [52]. For CETP inhibition the predicted decline in LDL-C as the fold-change in HDL-C increases is in good agreement with data on the three CETP inhibitors (Figure 13, panel E). Conversely for ABCA1 up-regulation the LMK model predicts an increase in LDL-C with increasing fold-change in HDL-C. This finding is a consequence of the first-order CETP-mediated transfer processes between HDL, VLDL and LDL particles. It is qualitatively consistent with the GWAS study of Voight *et al* [53] which showed that ABCA1 SNP rs3890182 raised HDL-C and LDL-C by comparable amounts.

Lipoprotein biomarkers

A number of studies have shown that CVD risk is correlated with plasma biomarkers such as HDL-C [1], HDL-P [54] and pre-β_1 [55,56] levels. In addition, the combination of NMR analysis of HDL with genotyping has also given a glimpse into the possible genes associated with HDL particle measures [57]. However, the mechanistic basis for these experimental observations as well as what underlies the correlations between the plasma biomarkers are not well understood. Using the proposed LMK model, we can reproduce and explain the correlations between these plasma biomarkers.

In addressing these questions, the simulated biomarkers within the population of 2000 virtual patients (as previously shown in Figure 7) were studied. The correlation between HDL-P and HDL-C within this set of virtual patients ($r=0.74$) is shown in Figure 14, panel A; we see that the simulation result is qualitatively similar to the positive correlation shown by Mackey *et al* [54] (the absolute values of HDL-P obtained by NMR are approximately 2-fold greater than our simulations which are based on the updated Shen model; the discrepancy is discussed in [25]). A positive correlation also exists in the virtual population between HDL size and HDL-C ($r=0.71$), consistent with Mackey *et al* [54] (see Figure 14, panel B).

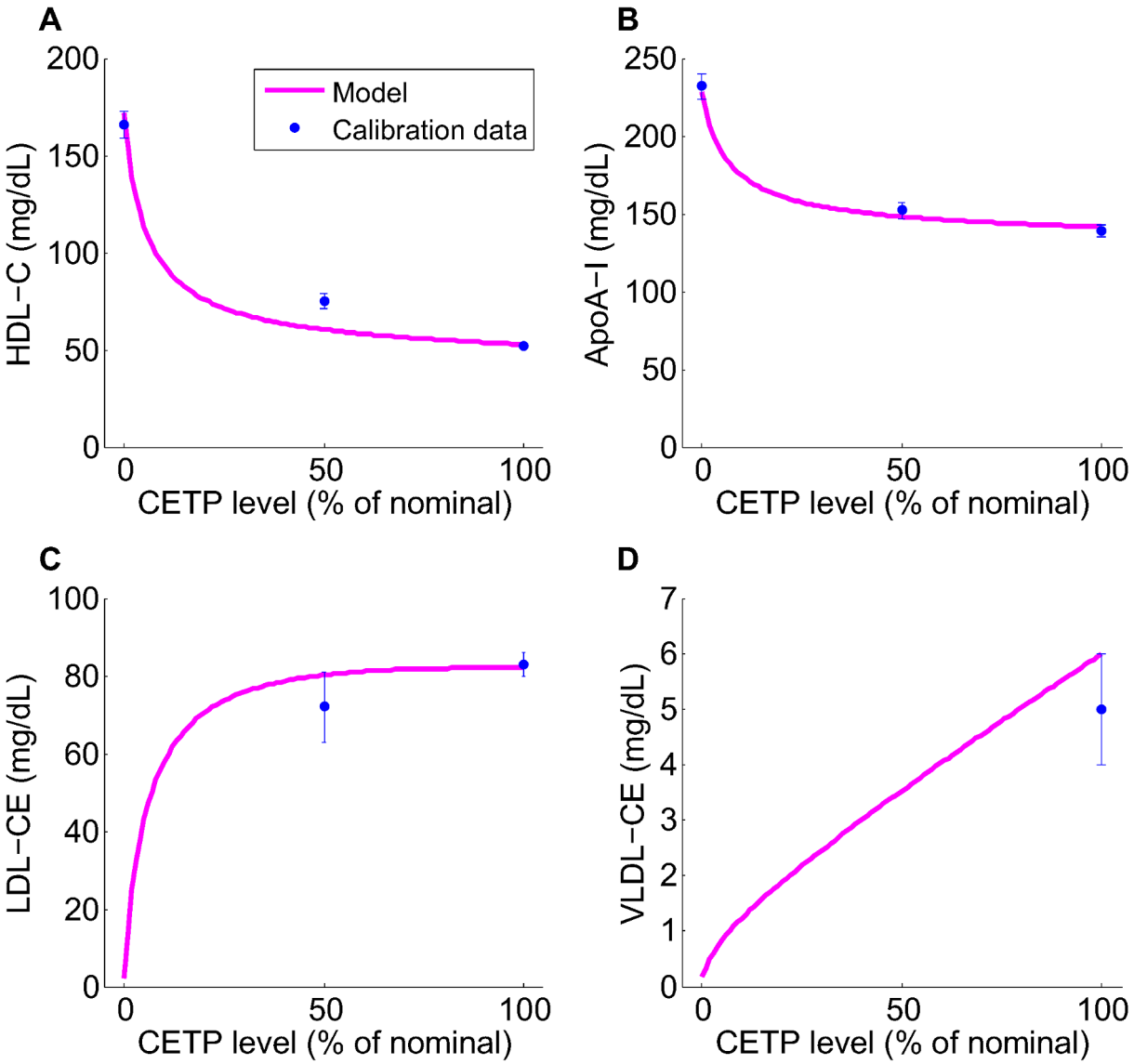

Figure 2. The fit of the model to the calibration data for CETP deficiency: HDL-C (panel A), ApoA-I (panel B), LDL-CE (panel C) and VLDL-CE (panel D). The data are as shown in Table 6, obtained by pooling HDL-C and ApoA-I data from references [81–83] and LDL-CE, VLDL-CE data from references [20,21]. The model simulation curves were obtained by decreasing the 3 parameters representing CETP activity (k_{HV}^{CETP},k_{HL}^{CETP},k_{LH}^{CETP}) from 100% to 0% of those corresponding to the nominal subject.
doi:10.1371/journal.pcbi.1003509.g002

Due to the growing appreciation for the importance of RCT [2,8,58], there are on-going efforts in trying to quantitatively assess the steps involved in the process. The ABCA1 transporter is involved in the first step of RCT by removing cholesterol from peripheral tissues to plasma and its activity level in patients has been studied [59]. In particular, ABCA1 gene expression and protein concentration on leukocytes has been measured in patients with type 2 diabetes, where the data suggested a negative correlation between ABCA1 expression and HbA1c levels [59]. While there are assays that can quantify ABCA1 protein levels in specific cell types [60], an experimental technique for the assessment of ABCA1 activity *in-vivo* at the whole body level has yet to be developed. Given the current experimental limitations, there is an interest to evaluate the potential effectiveness of plasma-based biomarkers for quantitatively assessing ABCA1 activity.

Using the LMK model, we evaluated the potential effectiveness of two biomarkers for ABCA1 activity: firstly, the absolute concentration of lipid-poor ApoA-I; secondly, the relative concentration of lipid-poor ApoA-I as the percentage of total ApoA-I. Figure 15 panel A shows that the former is only weakly correlated with ABCA1 activity. In contrast, panel B shows that the latter exhibits a strong inverse correlation with ABCA1 activity; in fact, given a measured value of % lipid-poor ApoA-I, the relationship can be used to estimate ABCA1 activity. This result can be better understood by the following analysis. From equation (1a), the absolute concentration of lipid-poor ApoA-I at steady state can be expressed as:

$$A_{lp} = \frac{r_{\text{in}}^{lp} + k_{\text{dissoc}} F\text{rem}(\text{CE}_\alpha, A_\alpha, N_\alpha)}{k_{\text{kidney}} + k_{\text{ABCA1}}} \qquad (4a)$$

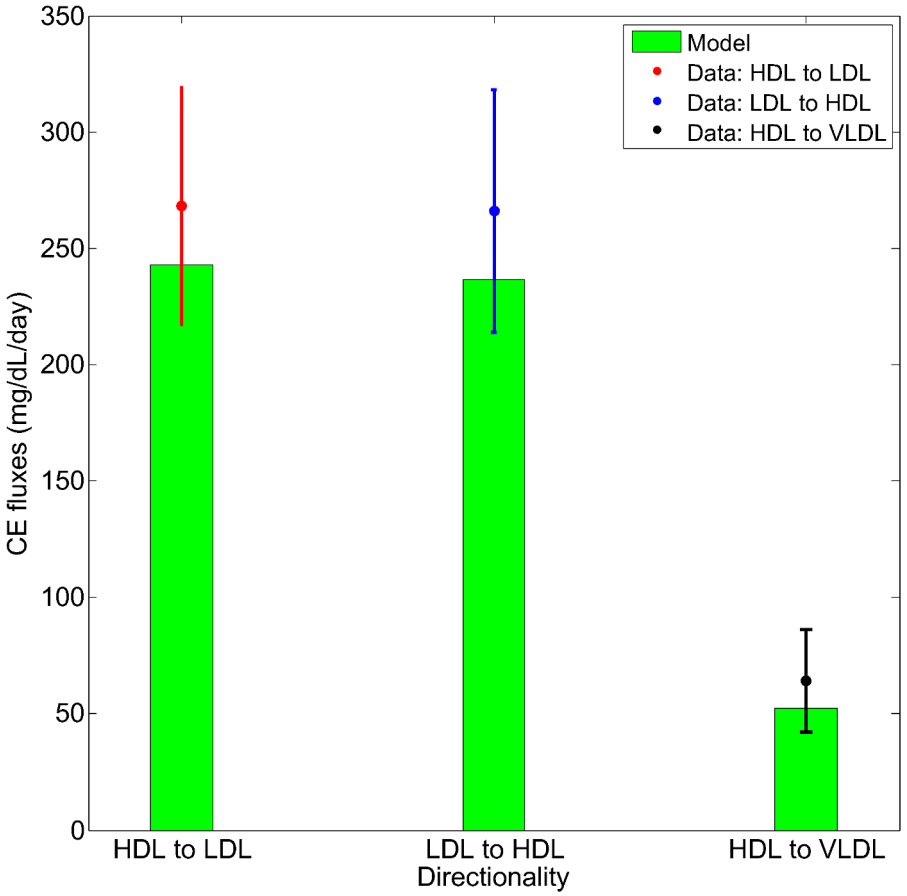

Figure 3. The fit of the model to the calibration data: CE fluxes. The data are as shown in Table 8, taken from reference [20]. The model simulation is produced using the point estimate of parameters for the nominal subject.
doi:10.1371/journal.pcbi.1003509.g003

$$\approx \frac{k_{\text{dissoc}} F\text{rem}(\text{CE}_\alpha, A_\alpha, N_\alpha)}{k_{\text{ABCA1}}}. \quad (4b)$$

On the other hand, from (1b) the % lipid-poor ApoA-I can be expressed as the following:

$$\frac{A_{lp}}{A_\alpha} = \frac{k_{\text{holo}}(d) + k_{\text{dissoc}} F\text{rem}(\text{CE}_\alpha, A_\alpha, N_\alpha)/A_\alpha}{k_{\text{ABCA1}}} \quad (5a)$$

$$\approx \frac{k_{\text{dissoc}} F\text{rem}(\text{CE}_\alpha, A_\alpha, N_\alpha)/A_\alpha}{k_{\text{ABCA1}}}. \quad (5b)$$

Comparison of the denominators in (4a) and (5a) show that in the former expression, an additional parameter k_{kidney} enters; however, it is small compared to k_{ABCA1} (the mean values being 2.42 and 95.18 respectively; see Table 5). In the numerator, the main quantitative difference between the two expressions is the remodeling flux, $k_{\text{dissoc}} F\text{rem}(\text{CE}_\alpha, A_\alpha, N_\alpha)$, versus the ApoA-I normalized flux, $k_{\text{dissoc}} F\text{rem}(\text{CE}_\alpha, A_\alpha, N_\alpha)/A_\alpha$. As shown in Figure 16, the latter has a flatter dependence on k_{ABCA1} as well as less variability due to other parameters. As a result, the ratio A_{lp}/A_α allows for a more precise estimate of k_{ABCA1} compared to A_{lp} above. In conclusion, the analysis shows that the stronger inverse relationship shown in Figure 15 panel B can be attributed to the normalization of the remodeling flux by ApoA-I.

The simulation results may further explain why, in some literature studies, % lipid-poor ApoA-I (note that the absolute concentration of lipid-poor ApoA-I can be experimentally estimated by assays that measure pre-β_1 [61]) has been proposed as a risk factor, as well as how increased % lipid-poor ApoA-I could be associated with CVD risk. Our proposal of using the % lipid-poor ApoA-I as a surrogate measure for ABCA1 activity is in concordance with the previous suggestion by Asztalos *et al* [62] that the ratio pre-β_1/α_1 is a measure of the efficiency of RCT: a decrease in this ratio has been thought to reflect an enhanced RCT [62,63]. In addition, our finding of the inverse correlation between % lipid-poor ApoA-I and ABCA1 activity may explain the observation that increased fractional pre-β_1 is associated with increased maximum intima-media thickness in both diabetics [64] and non-diabetic subjects [65], as well as being associated with an increased risk for coronary heart disease and myocardial infarctions [66].

Future directions

We foresee a number of potential future applications of the LMK model in the context of drug discovery and development, including the following:

1. Confirmation of a molecule's mechanism of action: this can be done by checking the clinically observed changes in lipoprotein

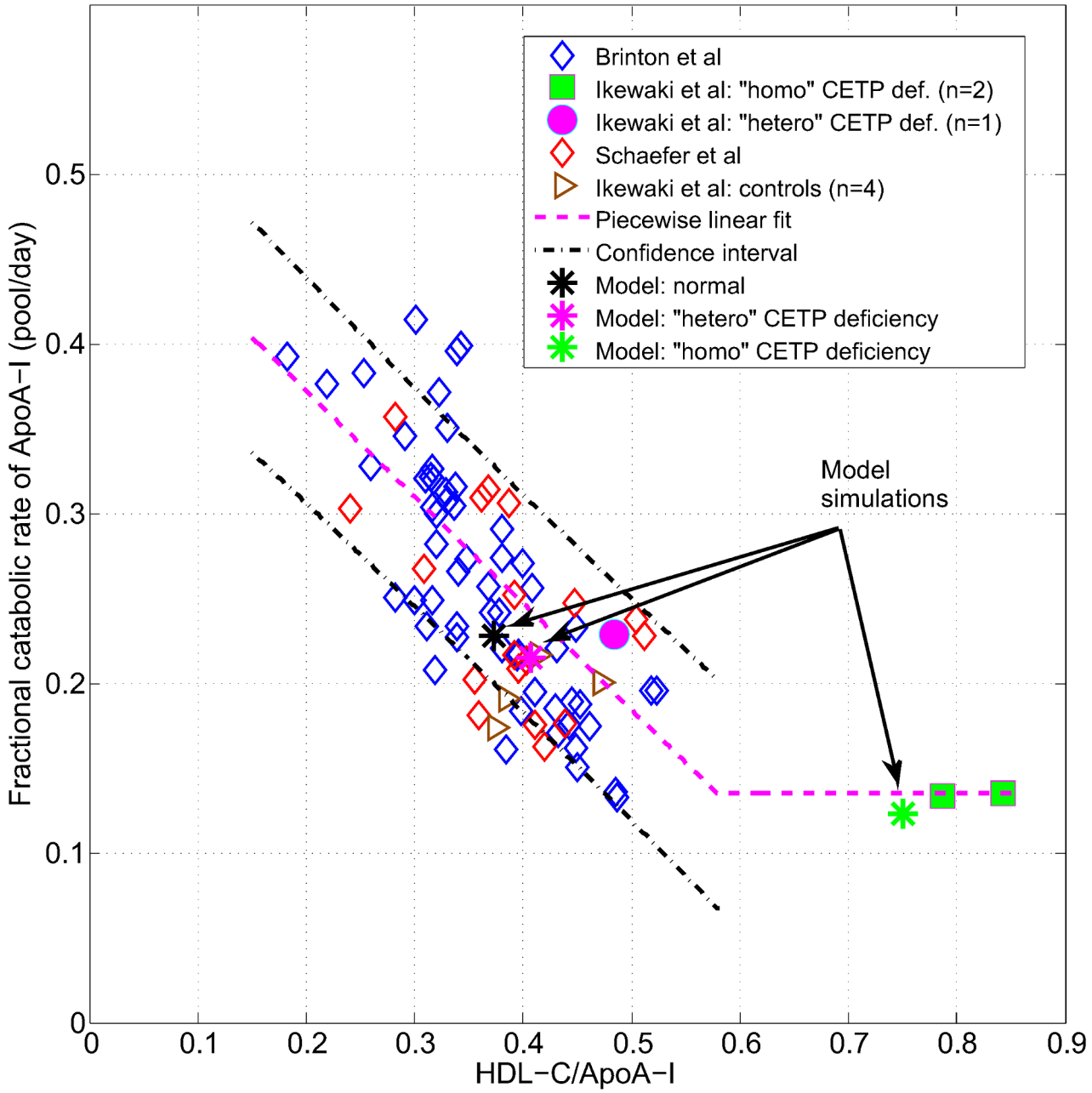

Figure 4. The fit of the model to the calibration data: FCR of ApoA-I versus HDL-C/ApoA-I ratio. The data sources are: Brinton *et al* [43], Ikewaki *et al* [45], Schaefer *et al* [44]. The piecewise linear fit and the confidence interval are discussed in the Methods section. The model simulation values are indicated by asterisk symbols, for the nominal subject and the heterozygote, homozygote of CETP mutation.
doi:10.1371/journal.pcbi.1003509.g004

measures against the model predictions. This is an important task, since a molecule that increases HDL-C may do so by modulating the RCT pathway not only on its intended target but may also have off-target effects. As the model shows, the choice of mechanism in raising HDL-C could be crucially important for whether or not it brings about cardiovascular benefit.

2. Determining the right dosage schedule for maximum cholesterol removal: the LMK model could help to integrate the pharmacokinetics of a molecule with the dynamics of HDL metabolism.
3. Evaluating combinations of target modulations: the LMK model could help to address the question of the potential synergism between targets in the RCT pathway.
4. Development of personalized health care (PHC) strategy: simulations of the model to generate virtual populations could be used to address the question of which patient subpopulations are most likely to benefit from a given therapy and how those subjects might be selected using plasma-based diagonostic tests.

The LMK model is focused on capturing the dynamics of ApoA-I and CE transfers. However, extensions of the model to incorporate ApoA-II dynamics as well as explicitly representing triglyceride and phospholipid metabolism would be important for describing the effects of other drug classes, including the PPAR-α and γ agonists [67,68] or synthetic phospholipids [69,70]. These remain topics for further research.

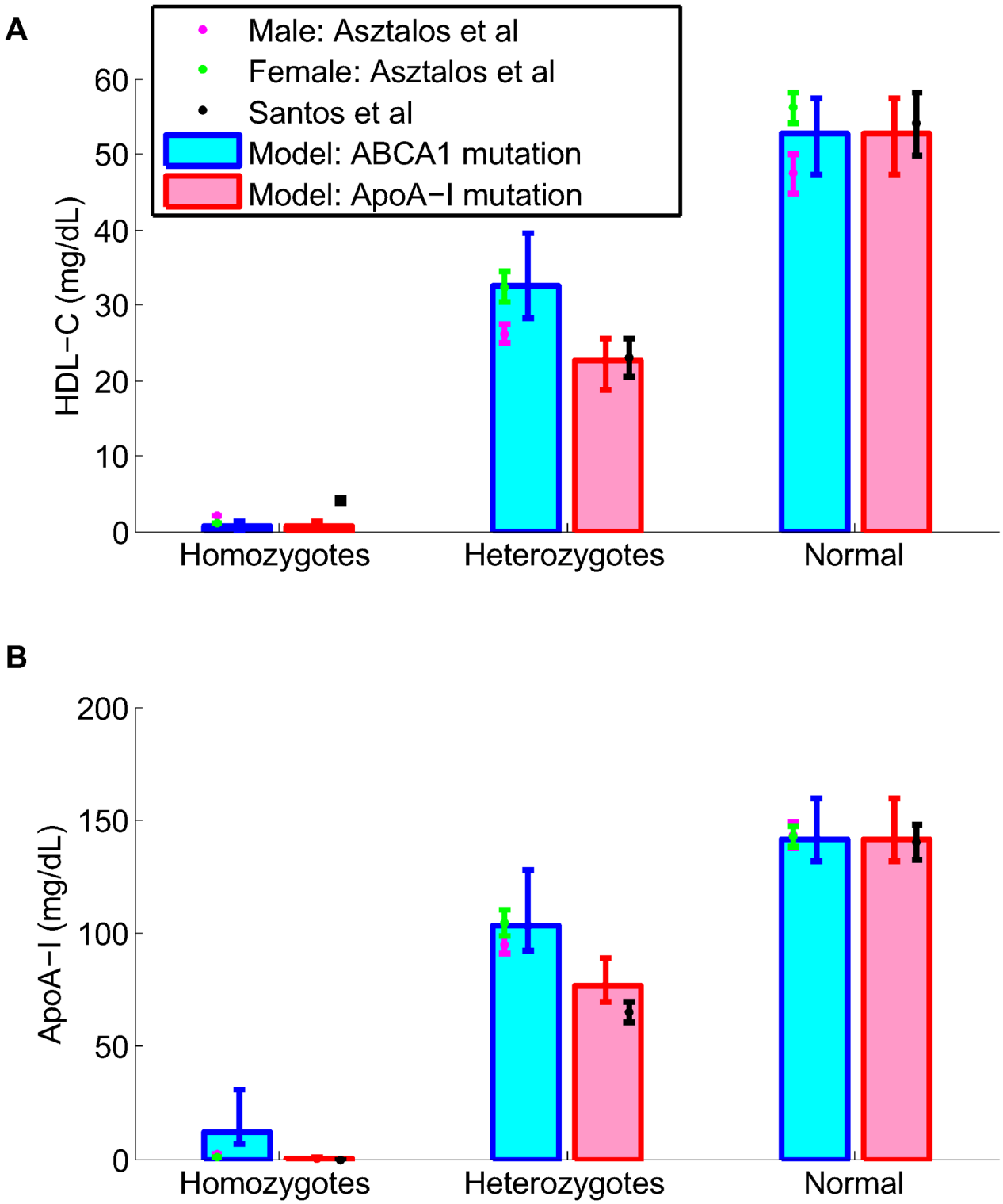

Figure 5. Model validation: simulation of ABCA1 and ApoA-I mutations compared with literature data for HDL-C (panel A) and ApoA-I (panel B). For the simulation results, the mean and the 95% confidence intervals are plotted. The data sources are Asztalos *et al* [46] and Santos *et al* [47]; the mean $\pm$ SD are shown. The model simulations of the mutation cases were obtained by taking the parameter values for the nominal subject and set k_{ABCA1} and r_{in}^{lp} to 50% and 0% of the nominal values respectively.
doi:10.1371/journal.pcbi.1003509.g005

Conclusions

We have developed a novel, *in-silico* model of lipoprotein metabolism focused on the reverse cholesterol transport pathway. The model incorporates important concepts of HDL biology, including the regeneration of lipid-poor ApoA-I via α-HDL remodeling processes, and has been calibrated using literature data

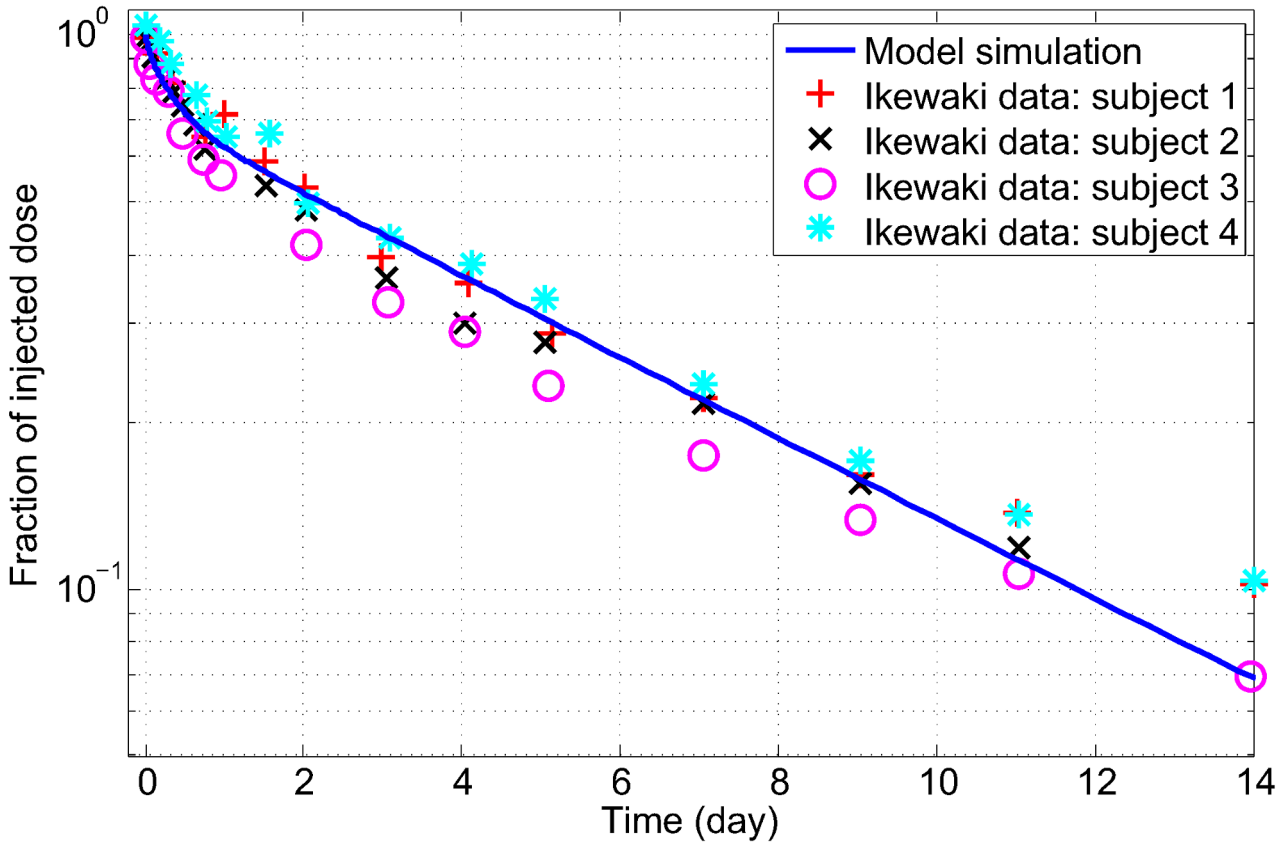

Figure 6. Model validation: Simulation of tracer kinetic experiment with labelled ApoA-I compared to experimental data. The data are obtained by digitization of tracer kinetics measurements carried out in 4 subjects and shown in Figure 3 of Ikewaki *et al* [48]. The model simulation corresponds to the nominal subject.
doi:10.1371/journal.pcbi.1003509.g006

from a wide variety of sources. The model has been further validated by simulating scenarios not considered in the calibration process. These include its ability to reproduce the levels of HDL-C and ApoA-I in hetero- and homozygous subjects with either ABCA1 or ApoA-I mutation and the observed biphasic kinetics of ApoA-I seen in tracer kinetics studies. This provides an increased confidence in the LMK model predictions with respect to modulations of these important targets and in the model's ability to simulate time-dependent scenarios.

In this paper, we have illustrated the applications of the LMK model in comparing the two target modulations, CETP inhibition and ABCA1 up-regulation. The results drawn from our model provide a possible explanation for the non-efficacy of dalcetrapib in the dal-OUTCOMES trial [7] as well as suggesting that ABCA1 is a target that would increase the RCT rate. The model provides predictions on the biomarker changes as a result of ABCA1 target modulation. Furthermore, computational experiments using a virtual population have shown why the % lipid-poor ApoA-I, rather than the absolute concentration of lipid-poor ApoA-I, is a better biomarker for assessing the *in-vivo* ABCA1 activity. By integrating mechanistic concepts and data, the model provides a way to quantitatively evaluate and explore hypotheses of lipoprotein metabolism.

Methods

Model derivation

Mass balance considerations. The LMK model (Figure 1) explicitly represents the mass balance of ApoA-I and CE molecules in plasma, whereas the mass balance of FC and PL molecules is represented implicitly. The input of ApoA-I to plasma reflects its synthesis rate, while the elimination of ApoA-I results from the excretion of lipid-poor ApoA-I by the kidney and holo-uptake of α-HDL particles by the liver. The remodeling of HDL particles by particle fusion, CETP, SRB1 and other processes leads to the recycling of ApoA-I from α-HDL particles to lipid-poor ApoA-I. Recycling influences the kinetics of ApoA-I in plasma but does not affect its mass balance. The input of CE to plasma reflects the rapid esterification of FC molecules in the nascent discs as they are converted to nascent spheres plus a small amount of CE which enters plasma during VLDL synthesis. The rate at which CE molecules appear in the α-HDL pool (via the nascent sphere) is defined in the LMK model as the RCT input rate and is assumed to equal the rate at which FC molecules are loaded onto the nascent discs (equation (2)). Elimination of CE from plasma results from holo-uptake and SRB1-mediated uptake of CE from all lipoprotein species. The CETP-mediated transfer of CE between α-HDL, VLDL and LDL does not affect the overall mass balance in plasma.

FC and PL molecules are present on the surfaces of all spherical lipoprotein particles in plasma as well as on the membranes of red blood cells (RBCs) and other cells that are in contact with the plasma. Based on Shen€s model of lipoprotein structure (Shen *et al* [71] and Mazer *et al* [25]), we assume that FC is in rapid equilibrium between all of these species and that the amount of FC present on each particle surface (at equilibrium) is dependent only on the surface curvature, that is, the radius of the hydrophobic

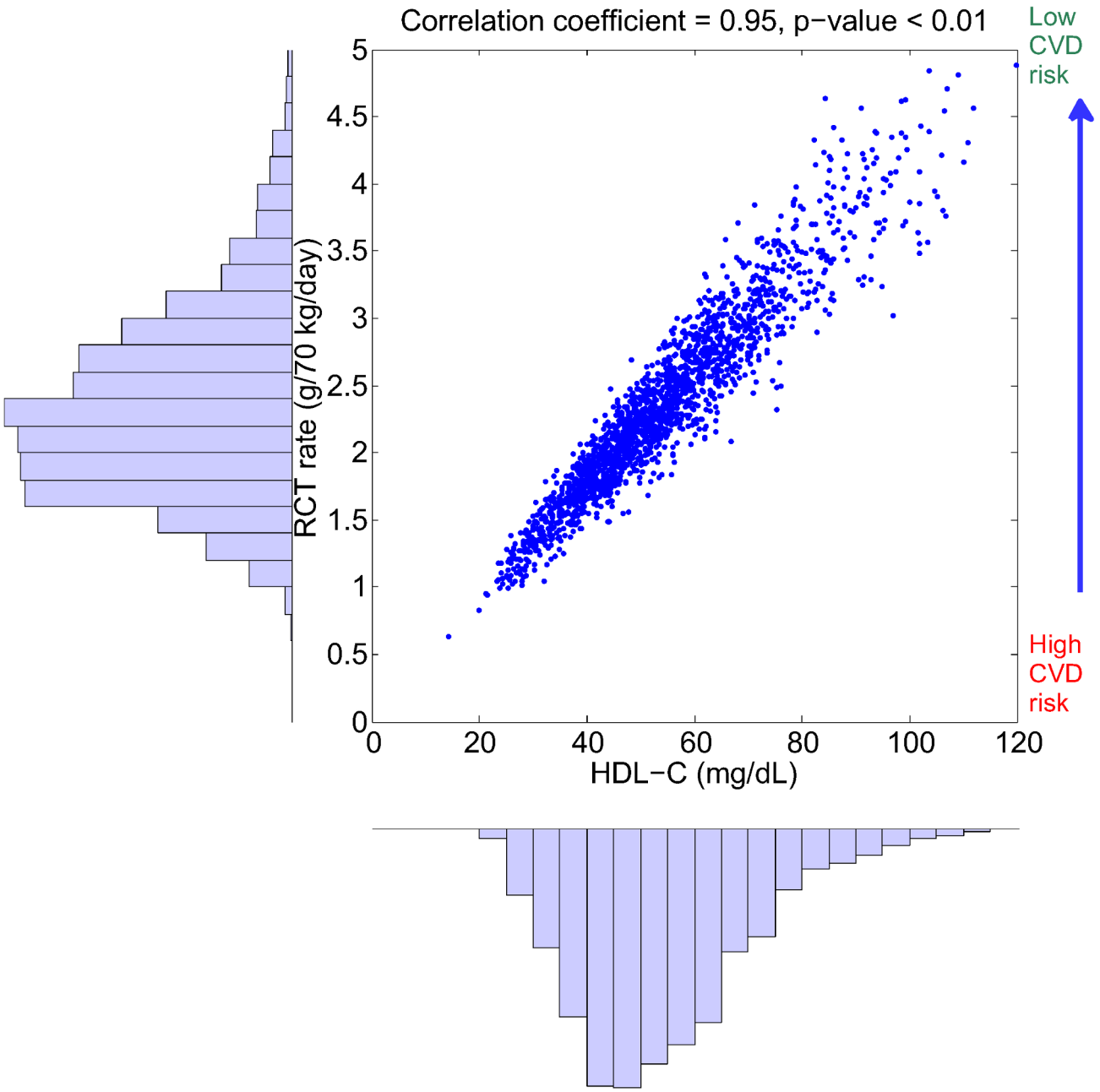

Figure 7. The distribution of RCT rate and HDL-C and their correlation in the simulated virtual population. By drawing the parameters of the model from an uncorrelated, multivariate normal distribution, a set of 2000 virtual patients is generated and the model simulations of RCT rate and HDL-C are shown. The right-hand axis represents the hypothetical inverse relationship between RCT rate and CVD risk.
doi:10.1371/journal.pcbi.1003509.g007

core of the particle (as represented in equation (10), below). The FC needed for the surface of the nascent spheres is assumed to be provided by the large pool of FC present in blood, including RBCs, and is largely replenished by the HDL remodeling processes. It can be shown that the rate at which FC is eliminated from plasma via holo-uptake of HDL particles is very small compared to the RCT rate (<4%) and is therefore negligible from the perspective of mass balance. Similar considerations apply to the mass balance of PL.

Particle size. The size of spherical α-HDL particles is computed in the model as follows. From the pool size of CE in α-HDL and the particle concentration, the number of CE molecules per HDL particle is given by:

$$n_{\mathrm{CE}}^{\mathrm{particle}} = \frac{\mathrm{CE}_{\alpha}(t)}{N_{\alpha}(t) m_C}. \tag{6}$$

Since CE_{α} is expressed as an equivalent mass of FC and m_C is the molecular weight of FC, $n_{\mathrm{CE}}^{\mathrm{particle}}$ is appropriately determined. With an assumed ratio of TG/CE = 0.13 in the core of HDL particles [25], we sum the volumes occupied by CE and TG to obtain the total core volume and determine the core radius (r_{core}) from it. Finally, the surface thickness $t = 20.2$ Å is added to the

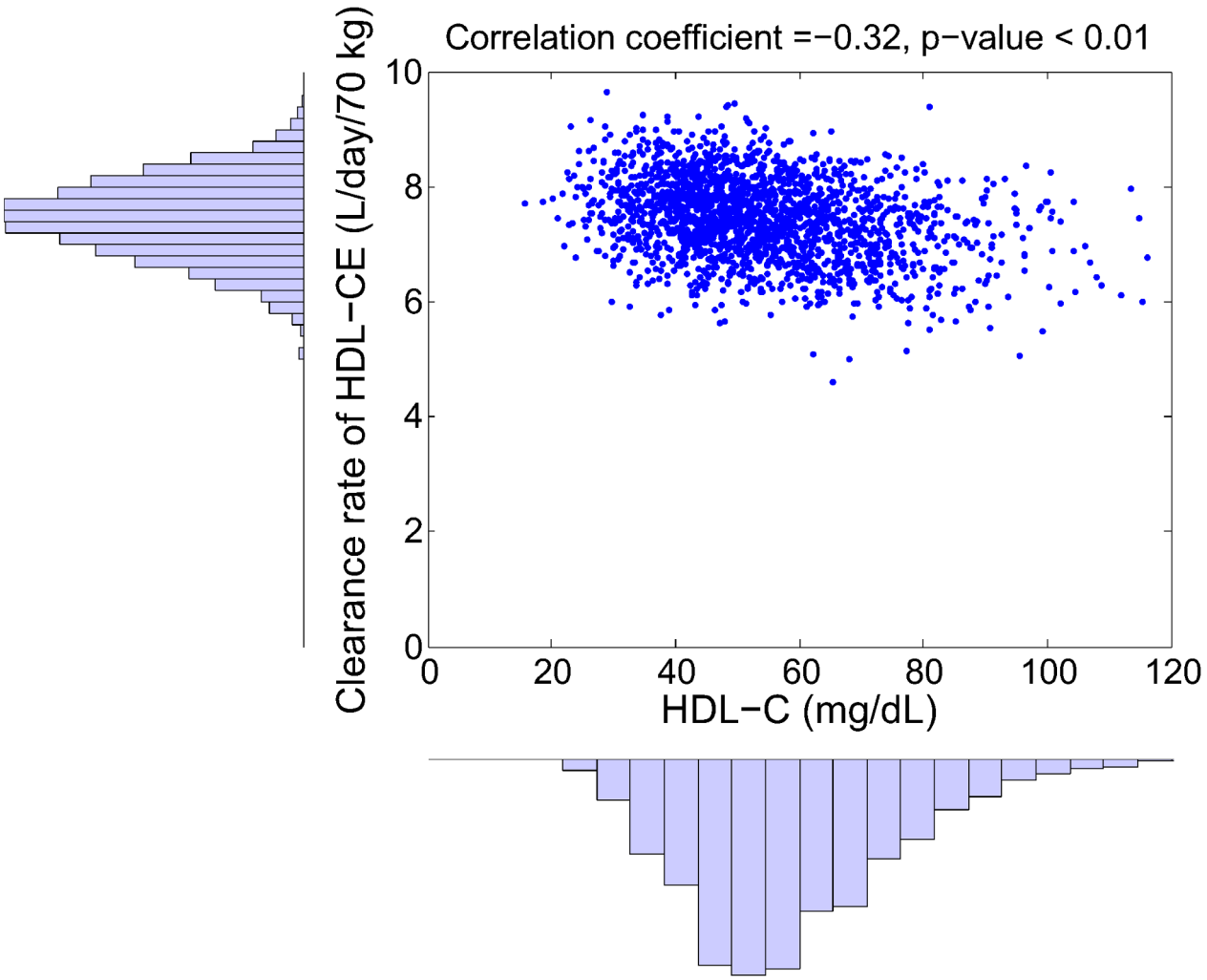

Figure 8. The distribution of the clearance of HDL-CE and HDL-C and their correlation in the simulated virtual population. By drawing the parameters of the model from an uncorrelated, multivariate normal distribution, a set of 2000 virtual patients is generated and the model simulations of HDL-CE clearance rate and HDL-C are shown.
doi:10.1371/journal.pcbi.1003509.g008

core radius, giving rise to following expression for the particle diameter, d (in Å):

$$r_{\text{core}} = \left(\frac{3}{4\pi} n_{\text{CE}}^{\text{particle}} \times (V_{CE} + 0.13 \times V_{TG})\right)^{1/3}, \quad (7)$$

$$d = 2 \times (r_{\text{core}} + 20.2). \quad (8)$$

Note that the molecular volumes V_{CE} and V_{TG} are defined in Table 3.

Remodeling flux. In the derivation of the remodeling flux, we compute the excess (or deficit) of ApoA-I compared to that derived using the updated Shen's model [25]. Given the pool size for $A_\alpha(t)$ and the particle concentration $N_\alpha(t)$, we compute the number of ApoA-I molecules per particle:

$$n_{\text{ApoA}-\text{I}}^{\text{particle}} = \frac{A_\alpha(t)}{N_\alpha(t) m_A}. \quad (9)$$

Using the expression for r_{core} given in (7), the number of ApoA-I molecules needed to cover the surface is derived in the following manner [25]: firstly, the number of free cholesterol is computed,

$$n_{\text{C}} = ((r_{\text{core}} + 20.2)^3 - r_{\text{core}}^3) \times \exp(-84.4/(r_{\text{core}} + 20.2) - 6.09). \quad (10)$$

Then, the number of phospholipid molecules needed to cover the remaining surface area of the core is computed:

$$n_{\text{PL}} = \frac{4\pi r_{\text{core}}^2 - n_{\text{C}} A_{\text{C}}}{A_{\text{PL}}}, \quad (11)$$

where the cross-sectional surface areas of cholesterol and phospholipid are $A_{\text{C}} = 39.1$ Å^2 and $A_{\text{PL}} = 68.5$ Å^2 respectively. The number of amino acids needed to cover the hydrophobic area exposed at the outer surface layer of HDL particle is:

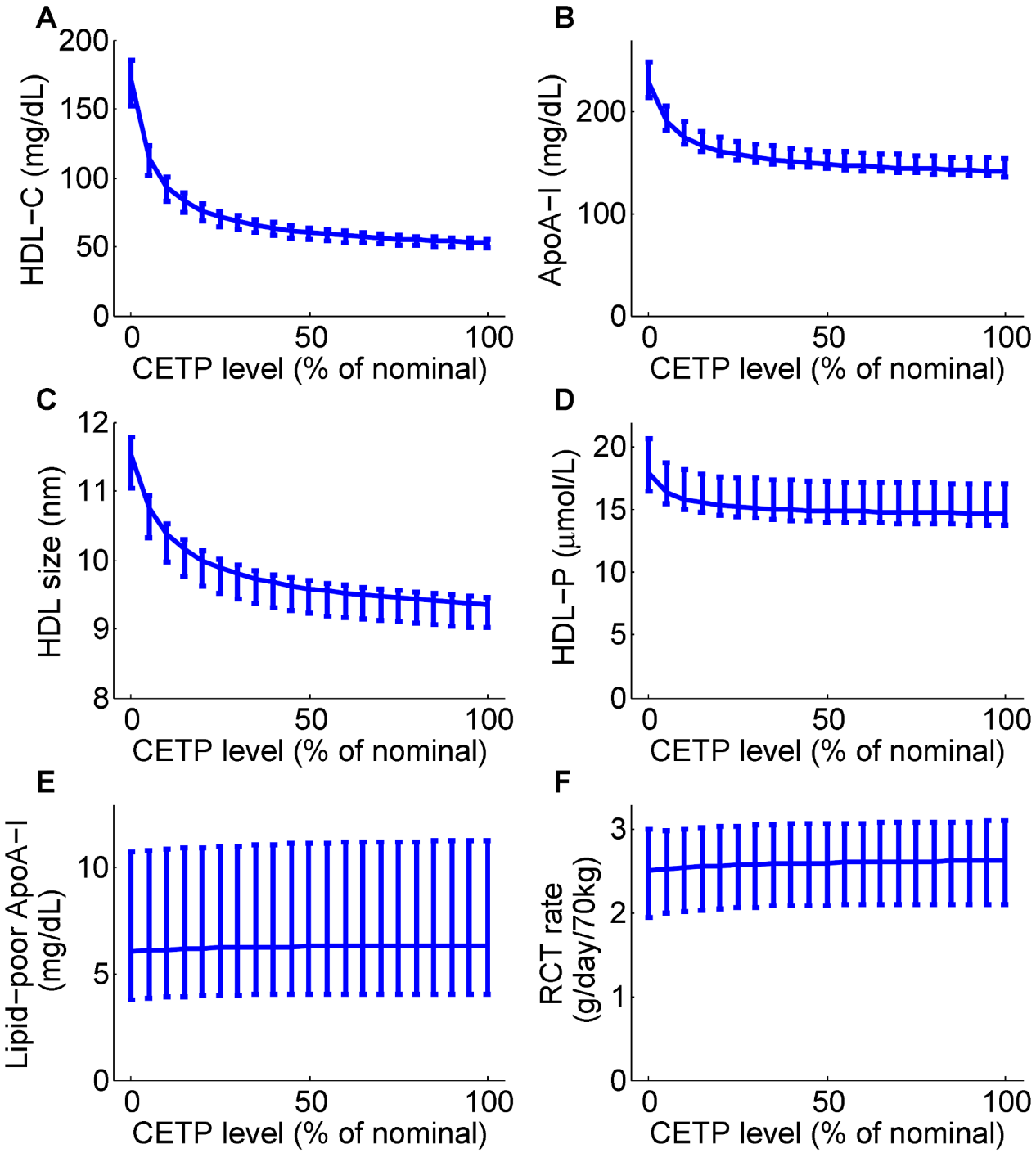

Figure 9. Model predictions for the dependence of HDL measures (HDL-C, panel A; ApoA-I, panel B; HDL size, panel C; HDL particle concentration, panel D; lipid-poor ApoA-I, panel E) and RCT (panel F) on the CETP level. The model simulation curves were obtained by decreasing the 3 parameters associated with CETP activity (k_{HV}^{CETP},k_{HL}^{CETP},k_{LH}^{CETP}) from 100% to 0% of those corresponding to the nominal subject. For each prediction, the mean and the 95% confidence intervals are plotted.
doi:10.1371/journal.pcbi.1003509.g009

$$n_{AA} = \frac{4\pi(r_{core}+20.2)^2 - n_{PL}A_{PL}}{A_{AA}}, \qquad (12)$$

where the cross-sectional area of an amino acid $A_{AA} = 15.6$ Å^2. Since there are 243 amino acids in ApoA-I, under the further assumption that the weight fraction of ApoA-I in the HDL proteome is 60% [25], the number of ApoA-I molecules needed to cover the surface of HDL is given by:

$$n_{ApoA-I}^{Shen} = \frac{n_{AA}\times 0.6}{243}. \qquad (13)$$

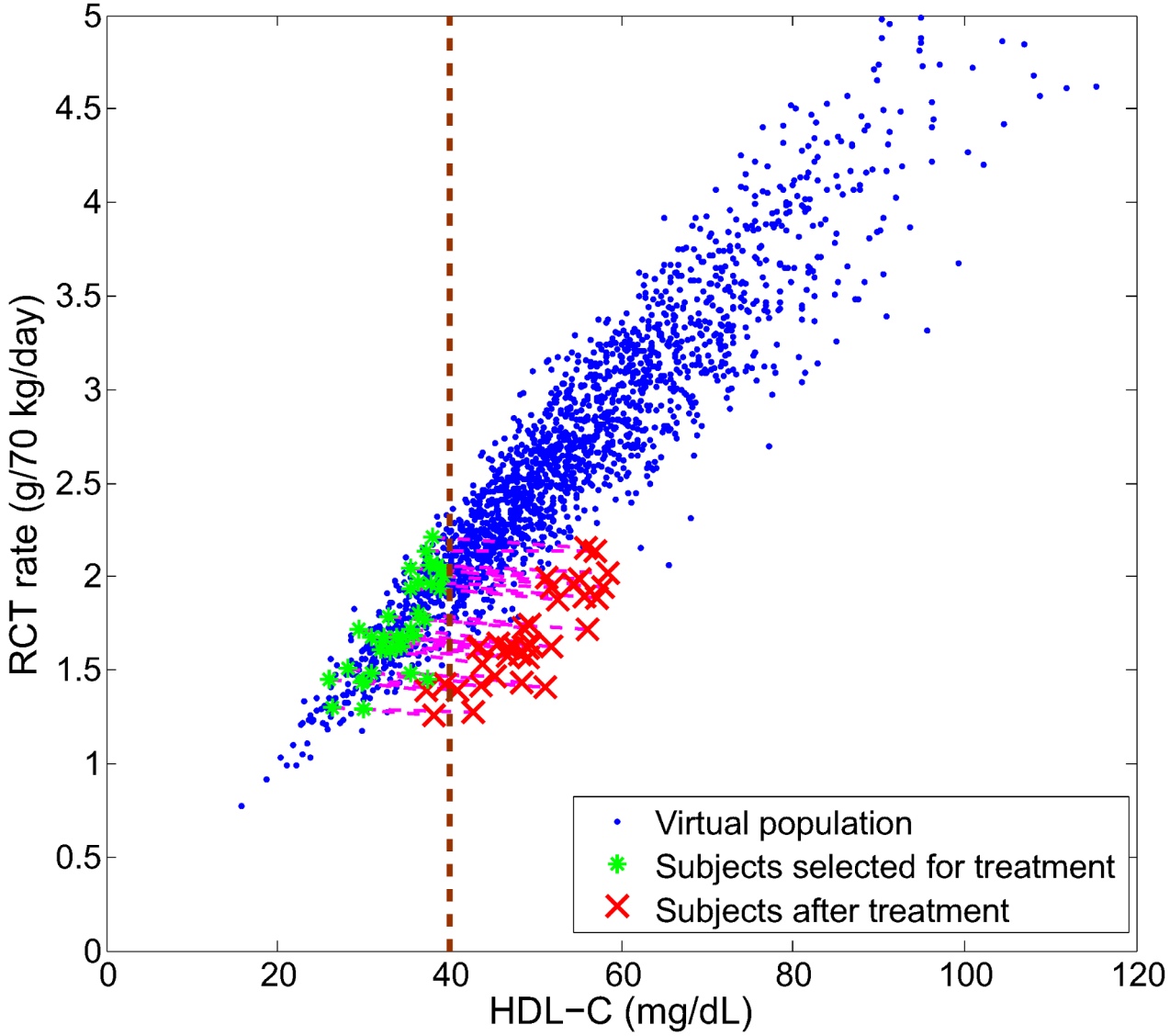

Figure 10. Simulation of CETP inhibition on a virtual population with low HDL-C (≤40 mg/dL). Each virtual patient selected for the treatment simulation had its rate constants associated with CETP activity ($k_{\mathrm{HV}}^{\mathrm{CETP}}$,$k_{\mathrm{HL}}^{\mathrm{CETP}}$ and $k_{\mathrm{LH}}^{\mathrm{CETP}}$) decreased to 20% of their original values.
doi:10.1371/journal.pcbi.1003509.g010

Finally, the discrepancy between the number of ApoA-I on the HDL (9) and the number needed from the Shen model (13), is the excess (or deficit) ApoA-I. Given the HDL particle concentration N_α, the following is the concentration of ApoA-I on α-HDL which is available to dissociate as the remodeling flux:

$$F_{\mathrm{rem}}(\mathrm{CE}_\alpha(t),A_\alpha(t),N_\alpha(t))= m_A \times N_\alpha \times \left(n_{\mathrm{ApoA-I}}^{\mathrm{particle}} - n_{\mathrm{ApoA-I}}^{\mathrm{Shen}}\right). \quad (14)$$

HDL holo-particle uptake. Our model allows for the possibility of a linear size dependence of the HDL holo-particle uptake rate. However, no prior assumption is made regarding the size dependency; using the calibration data, the sign and magnitude of the linear dependence is determined. In particular, the rate of holo-uptake has the following form, where the calculation of size d is given by equation (8) and the division by 10 accounts for the conversion from Å to nm:

$$k_{\mathrm{holo}}(d)=k_{\mathrm{holo}}^{c}+k_{\mathrm{holo}}^{l}\times\left(\frac{d}{10}-7\,\mathrm{nm}\right). \quad (15)$$

Parameter priors

In this section, prior estimates of model parameters are given, including references to the original literature and the rationale for the choice of prior and the level of uncertainty. In a manner similar to a previously proposed Bayesian approach [35], uncertainty is increased by a factor $\mu_{\mathrm{map}}=2$ in the following cases:

- quantities that are measured *in-vitro* and mapped to the *in-vivo* context;

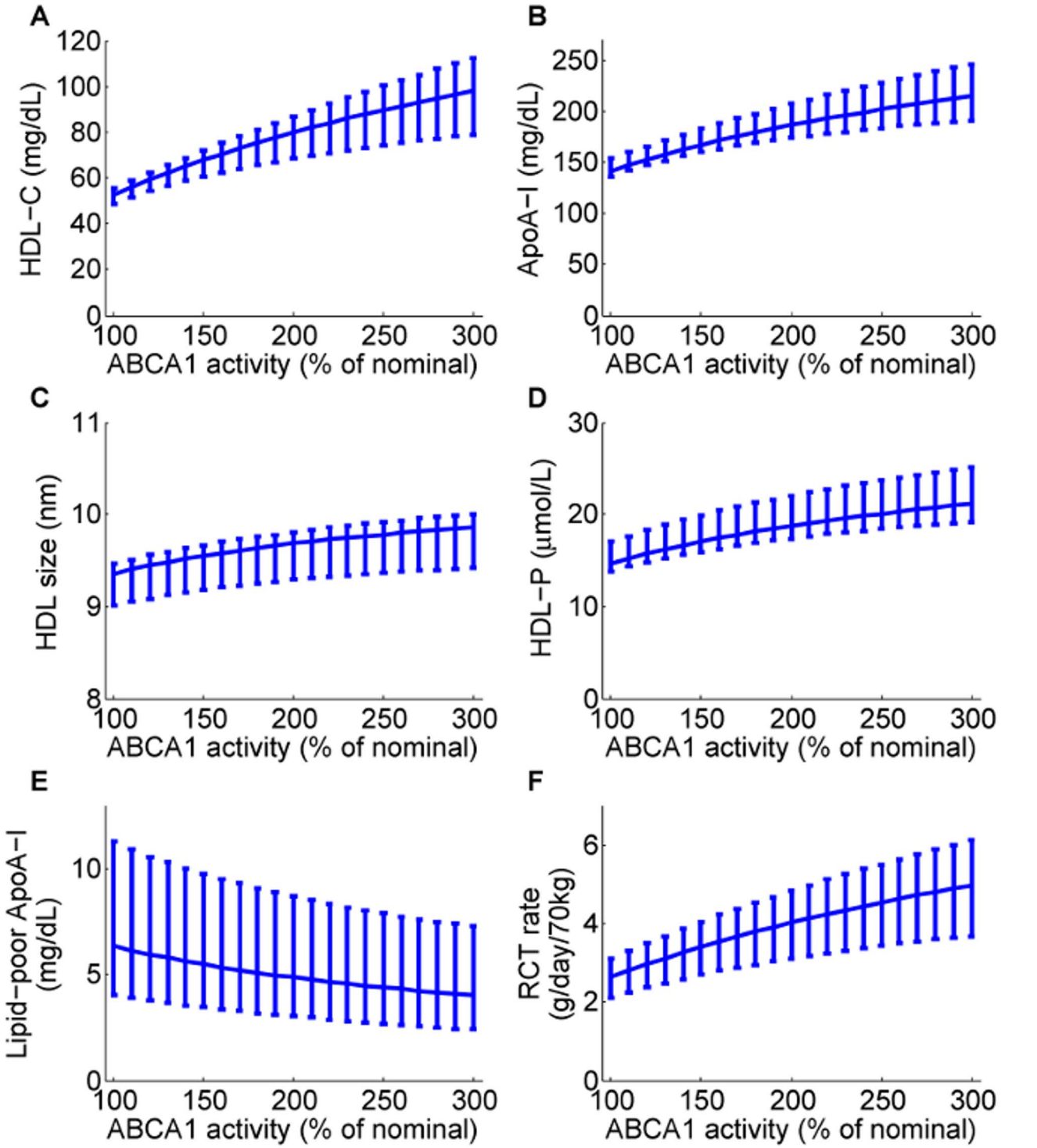

Figure 11. Model predictions for the dependence of HDL measures (HDL-C, panel A; ApoA-I, panel B; HDL size, panel C; HDL particle concentration, panel D; lipid-poor ApoA-I, panel E) and RCT (panel F) on ABCA1 activity. The model simulation curves were obtained by increasing the parameter representing ABCA1 activity (k_{ABCA1}) from 100% to 300% of the nominal subject. For each prediction, the mean and the 95% confidence intervals are plotted.
doi:10.1371/journal.pcbi.1003509.g011

- quantities that are measured in a population with mutation(s) and mapped to normal subjects;
- quantities that result from pooling data obtained using distinct experimental techniques/assumptions.

No explicit prior correlations are assumed.

Synthesis rate of ApoA-I (r_{in}^{lp}). The kinetics of ApoA-I were measured in $n = 20$ (11 males, 9 females) healthy subjects, with mean HDL-C = 46 mg/dL and ApoA-I = 115 mg/dL [44]. The

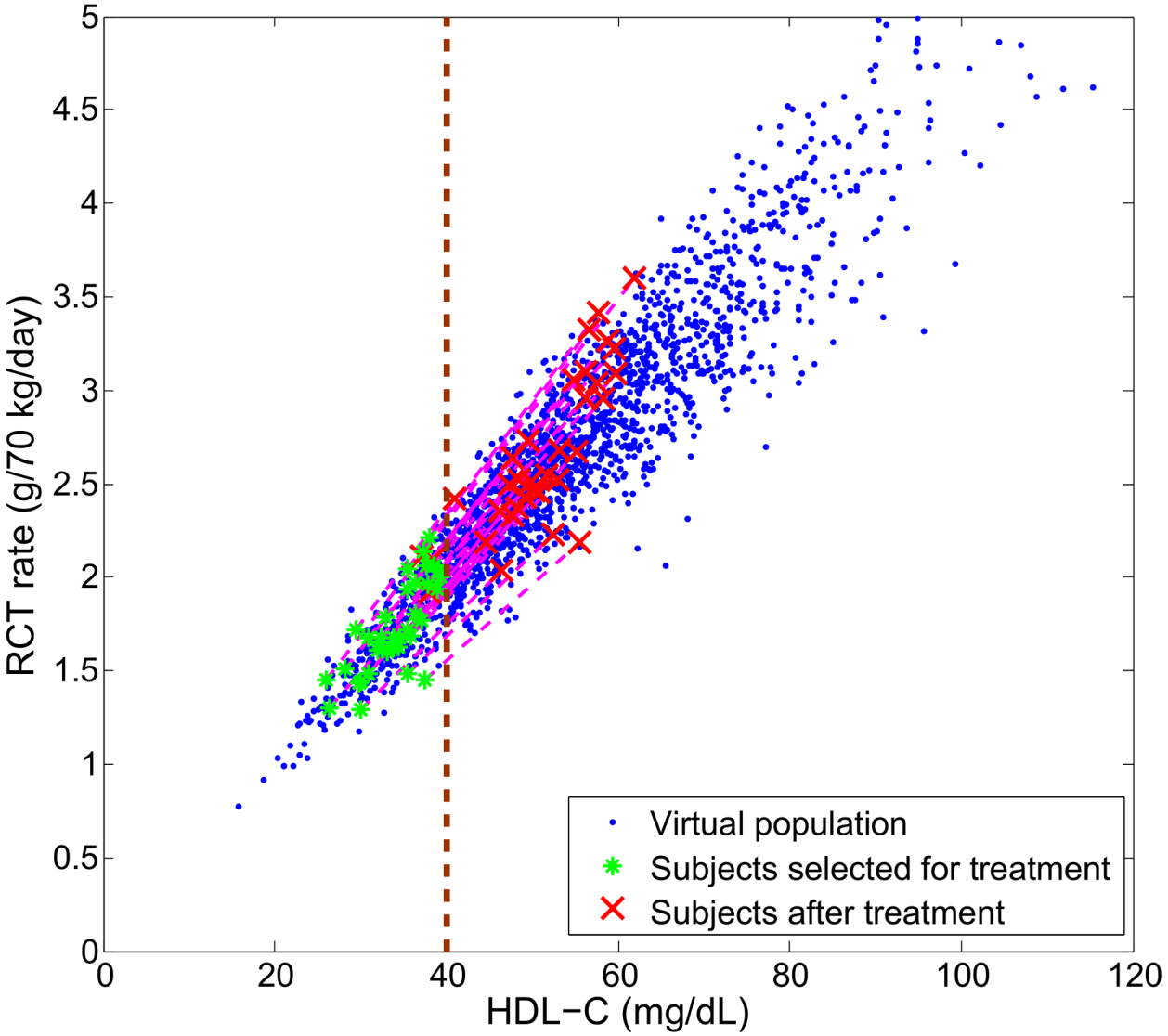

Figure 12. Simulation of ABCA1 up-regulation on a virtual population with low HDL-C (≤40 mg/dL). Each virtual patient seleted for the treatment simulation had its ABCA1 activity (k_{ABCA1}) increased by 100% of its initial value.
doi:10.1371/journal.pcbi.1003509.g012

ApoA-I synthesis rate has been estimated to be 27.44 ± 5.29 mg/dL/day (mean±SD). Hence, we take $r_{\mathrm{in}}^{lp} = 27.44 \pm 1.18$ mg/dL/day (mean±SEM).

Rate of kidney elimination (k_{kidney}). There have been a number of papers describing the measurement of the FCR of pre-β_1 [22,72]. However, the quantification of pre-β_1 can be a challenging task and a more direct assessment of the clearance rate of lipid-poor ApoA-I is estimated by the FCR of ApoA-I in Tangier patients. In the model representation of homozygous Tangier patients ($k_{\mathrm{ABCA1}} = 0$), the FCR of ApoA-I equals the kidney clearance of lipid-poor ApoA-I. The hypothesis that kidneys is responsible for a large fraction of ApoA-I clearance is supported by the study of Braschi *et al* done using rabbits [73], where it was estimated that the kidneys contribute around 70% of total ApoA-I clearance. The residence times (RT) of ApoA-I in Tangier disease patients have been measured to be 0.30,0.13 day in [74] and 0.22 day in [75]. It is assumed that in Tangier patients, $k_{\mathrm{kidney}} = 1/\mathrm{RT}$. Thus, k_{kidney} has been estimated to be 5.19 ± 1.30 pool/day (mean±SEM). Because of the assumption made in mapping ApoA-I clearance measured in the Tangier patients to the normal population, we apply the factor $\mu_{\mathrm{map}} = 2$ to give $k_{\mathrm{kidney}} = 5.19 \pm 2.60$ pool/day (mean±″ SEM).

Dissociation rate constant of labile ApoA-I (k_{dissoc}). In [76], fluorescence resonance energy transfer spectroscopy was used to quantify the rate of ApoA-I exchange. In this *in-vitro* set-up using synthetic rHDL incubated with 5-molar excess of lipid-free ApoA-I, the exponential relaxation time (defined as the time by which 50% of the exchange has occurred) was inferred to be 0.94 hour. This gives rise to the estimate of $k_{\mathrm{dissoc}} = 17.7$ pool/day [76]. The ApoA-I found on α-HDL particles can be divided into a tightly-bound pool [77] and a labile pool [78]. The study of the dissociation of ApoA-I molecules from the labile pool is carried out in [78], where surface plasmon resonance was used to study the kinetics of ApoA-I interaction with HDL particles. A two-state binding

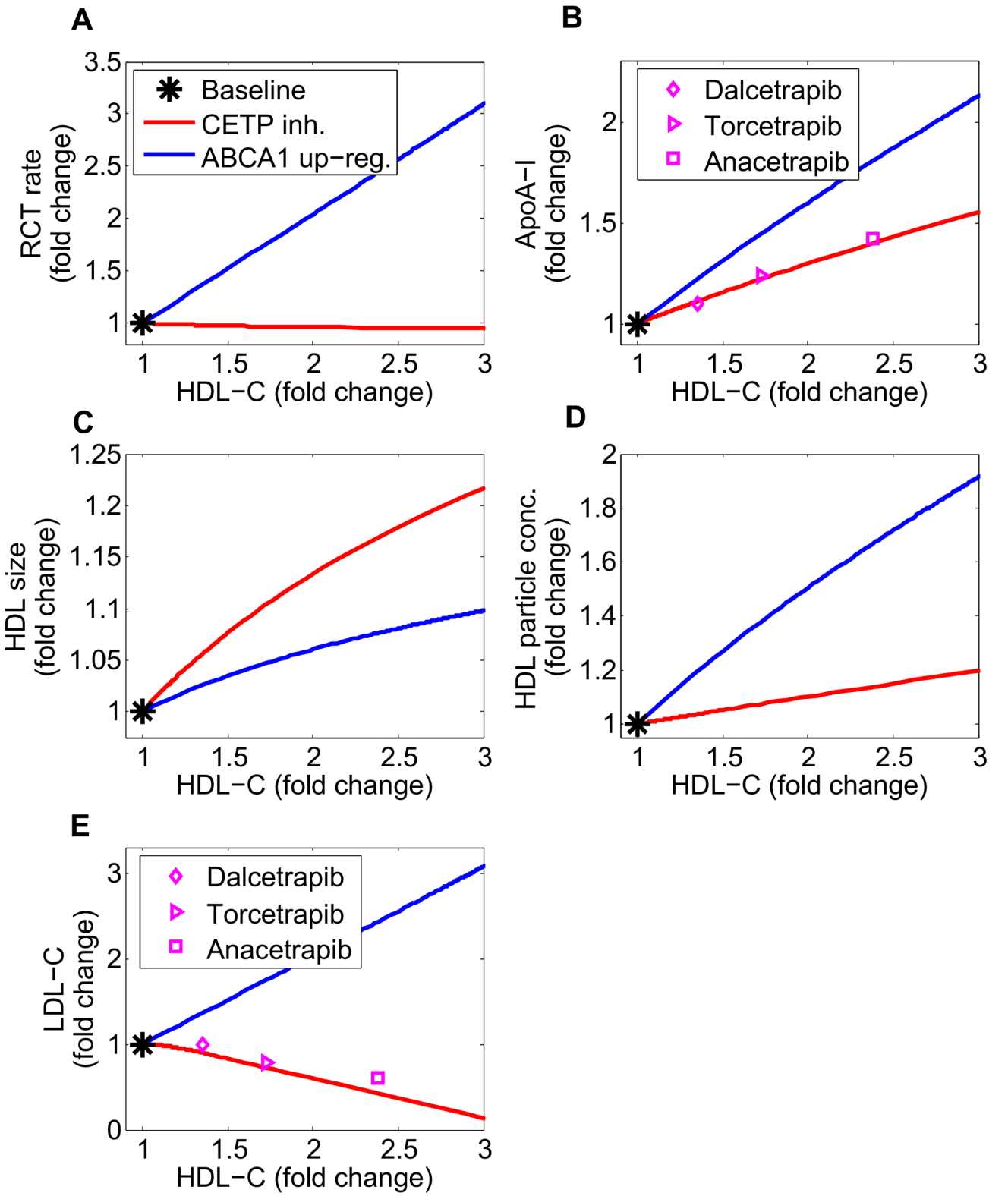

Figure 13. Comparison of CETP inhibition with ABCA1 up-regulation: changes in RCT rate (panel A) and biomarkers (ApoA-I, panel B; HDL size, panel C; HDL particle concentration, panel D; LDL-C, panel E) versus the rise in HDL-C. The nominal subject is taken as the baseline. The model simulation of CETP inhibition is compared with literature data of CETP inhibitors, Dalcetrapib [50], Torcetrapib [51] and Anacetrapib [52].
doi:10.1371/journal.pcbi.1003509.g013

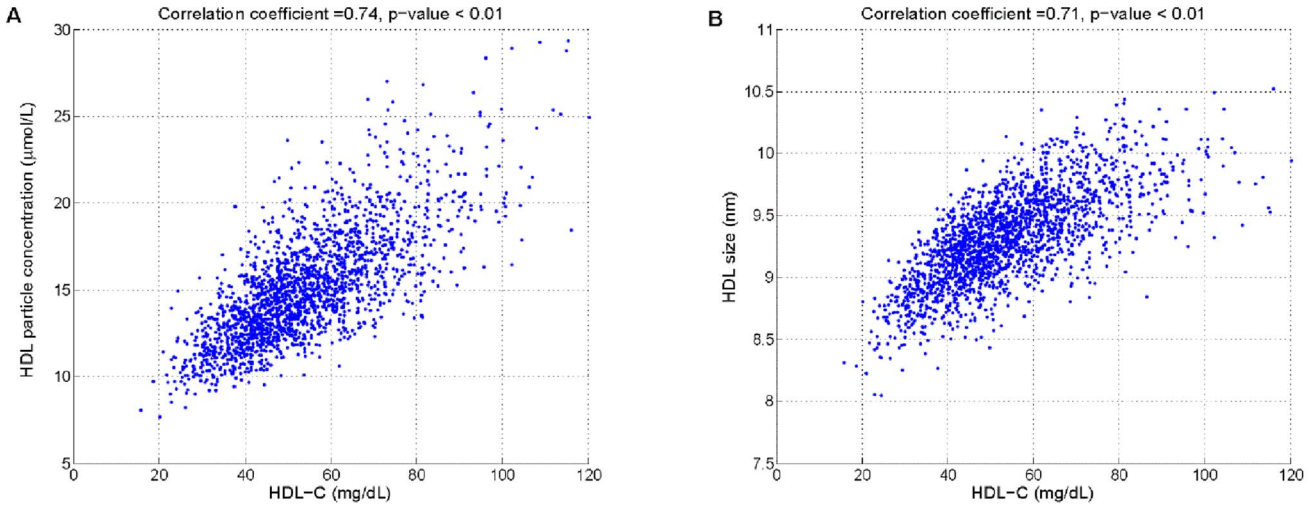

Figure 14. Correlations between HDL-C and HDL-P (panel A), and HDL-C and HDL size (panel B) in a virtual population of 2000 subjects.
doi:10.1371/journal.pcbi.1003509.g014

model was used to describe the association and dissociation reactions and the rate parameters were identified from the time-course data. It has been found that for the pool of ApoA-I molecules that are bound to HDL particles in a stable conformation, the half-time of dissociation is around 3 minutes, corresponding to $k_{\mathrm{dissoc}} \approx 330$ pool/day. Computing the mean and SD of the two estimates of k_{dissoc} and using $\mu_{\mathrm{map}} = 2$ to account for the fact that these values were measured *in-vitro*, we obtain $k_{\mathrm{dissoc}} = 174 \pm 312$ pool/day (mean$\pm$SEM).

Rate constant of the lipidation of lipid-poor ApoA-I via ABCA1 (k_{ABCA1}). The model assumes that the lipidation of ApoA-I is initiated by ABCA1, leading to the formation of nascent discs and subsequently to nascent spheres (via LCAT). While LCAT is crucial for the esterification of free cholesterol to cholesteryl ester, ABCA1 activity is assumed to be rate-limiting in the formation of α-HDL. In the model, the rate at which the concatenation of processes leading from lipid-poor ApoA-I to mature, α-HDL is described by the ABCA1 activity, k_{ABCA1}. Based on the size exclusion chromatographic technique for separating HDL into subclasses, the rate constant in the conversion of lipid-poor ApoA-I to the α-HDL pool has been estimated to be 96.24 ± 42.99 pool/day (mean$\pm$SD, n = 6) [22]. Thus, the mean and SEM is given by $k_{\mathrm{ABCA1}} = 96.24 \pm 17.55$ pool/day (mean$\pm$SEM).

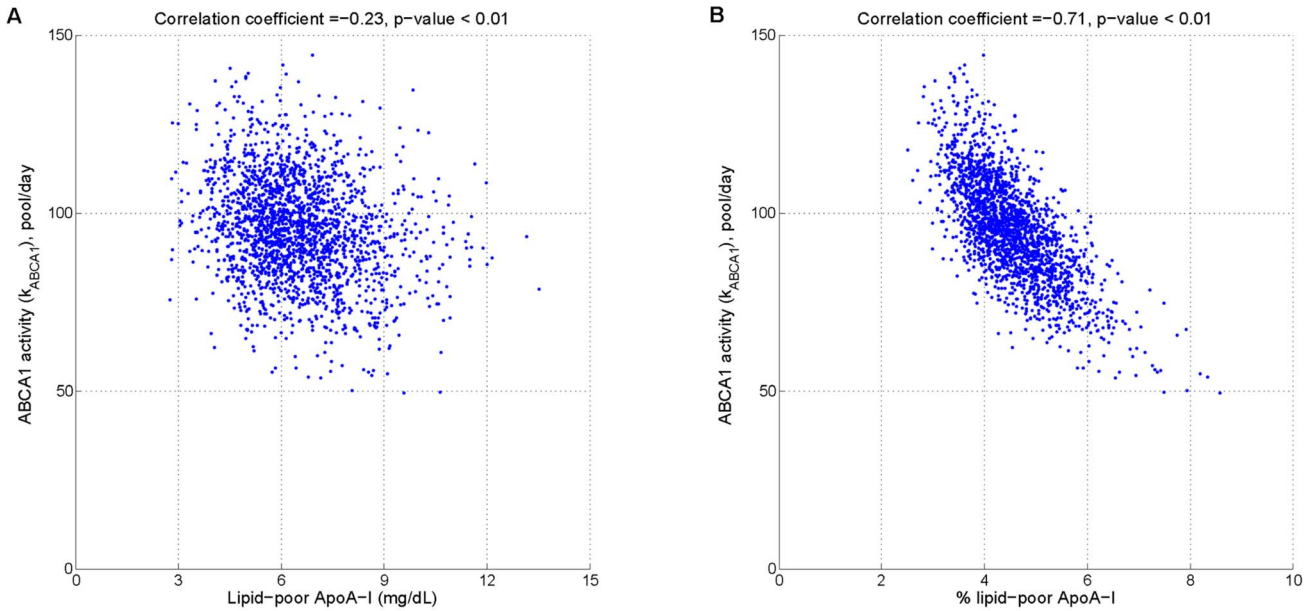

Figure 15. Correlations between k_{ABCA1} and absolute concentration of lipid-poor ApoA-I (panel A), and between k_{ABCA1} and % lipid-poor ApoA-I (panel B) in a virtual population of 2000 subjects.
doi:10.1371/journal.pcbi.1003509.g015

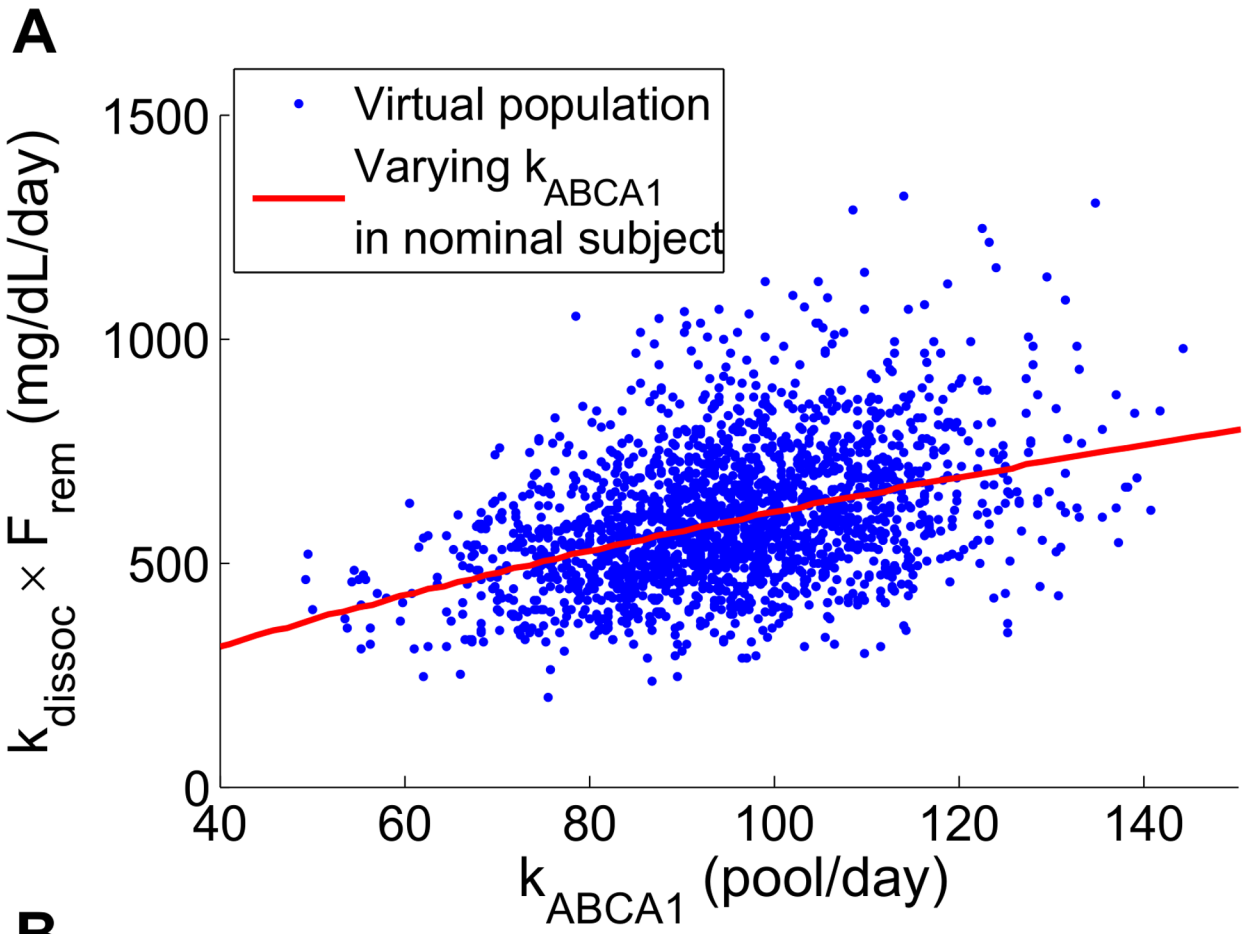
A
Virtual population
Varying k_{ABCA1}
in nominal subject
$k_{dissoc} \times F_{rem}$ (mg/dL/day)
1500
1000
500
0
40
60
80
100
120
140
k_{ABCA1} (pool/day)

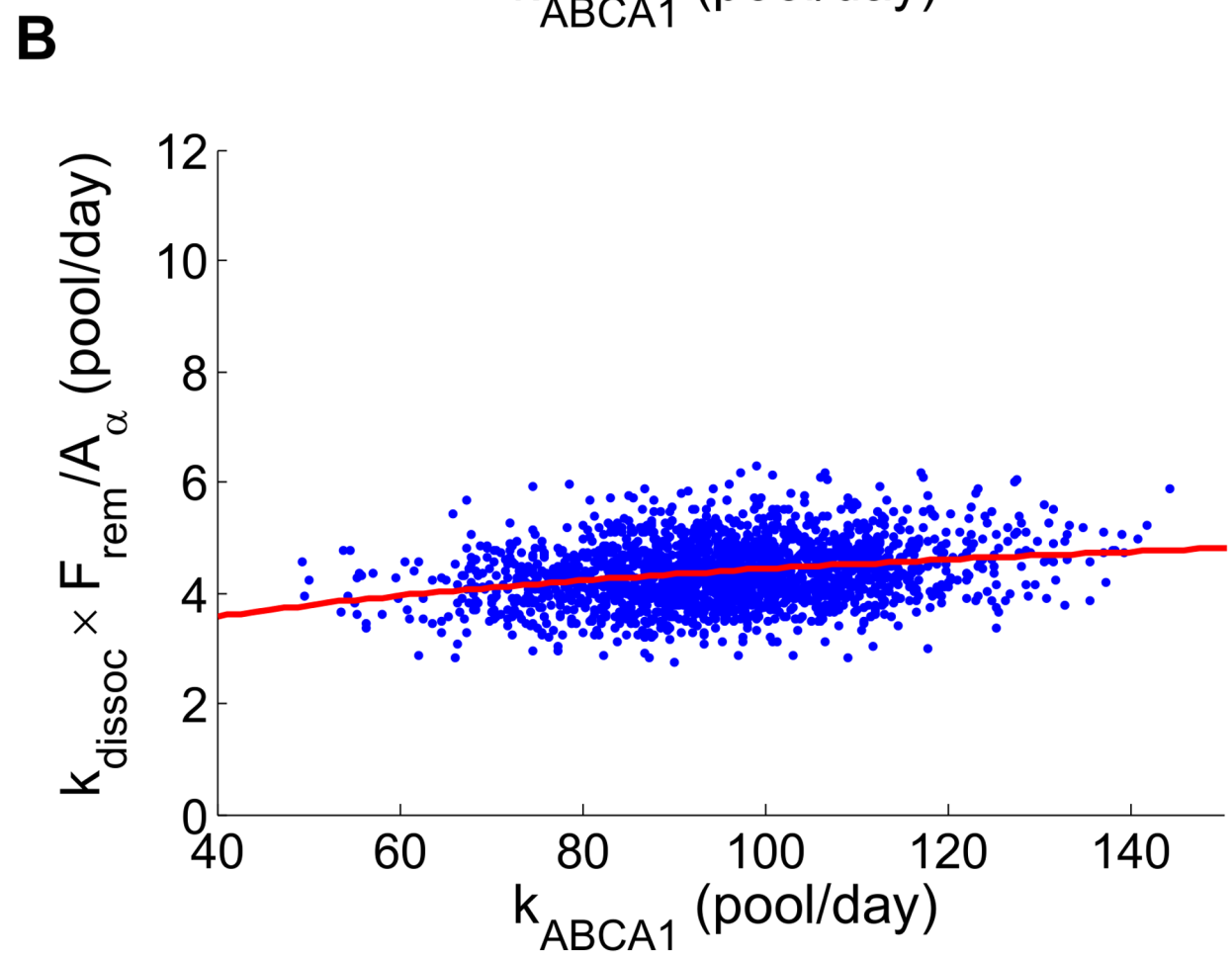
B
$k_{dissoc} \times F_{rem}/A_{\alpha}$ (pool/day)
12
10
8
6
4
2
0
40
60
80
100
120
140
k_{ABCA1} (pool/day)

Figure 16. Comparison of two expressions involving remodeling flux: $k_{\mathrm{dissoc}} \times F_{\mathrm{rem}}$ (panel A) and $k_{\mathrm{dissoc}} \times F_{\mathrm{rem}}/A_{\alpha}$ (panel B). The distributions of absolute and ApoA-I adjusted remodeling flux in the virtual population are plotted against k_{ABCA1}. The simulations of the nominal subject with only the parameter k_{ABCA1} varied are shown as solid lines.
doi:10.1371/journal.pcbi.1003509.g016

Stoichiometry of FC to ApoA-I in nascent discs (γ). In the model, γ denotes the stoichiometry (or molar ratio) of FC to ApoA-I in nascent discs. Due to the model assumption that FC in nascent discs are all esterified and result in the formation of nascent spheres, γ also equals the stoichiometry of CE to ApoA-I entering the α-HDL pool. Given these two interpretations of the model parameter γ, there are alternative ways to estimate it from literature data. In [79], plasma was fractionated using two-dimensional electrophoresis and the composition of pre-β_1 was analyzed. The weight fraction of FC to ApoA-I was found to be 0.16 ± 0.04 (n = 4). Using the given molecular weights of ApoA-I and FC, we obtain the molar ratio of FC/ApoA-I = 11.7 ± 1.5 (mean±SEM). An alternative estimate of γ is obtained using the estimates for the rate of cholesterol esterification to HDL-CE (77.2 ± 12.5 mg/dL/day, $n = 3$) [20] as well as the production rate of α-HDL from pre-β_1 (882 ± 540 mg/dL/day, $n = 6$) [22]. Thus, using these sets of data γ is estimated to be 6.46 ± 2.22 (mean ± SEM). Finally, an *in-vitro* experiment has been carried out to characterize the composition of nascent HDL (nHDL) formed by the action of ABCA1 on ApoA-I [80]. For the small nHDL formed (diameter ≈7.5 nm), the particles were found to contain, on average, 2 ApoA-I and 9 total cholesterol. This gives the estimate for γ of 4.5. Thus, combining all three estimates we get $\gamma = 7.55 \pm 1.97$ (mean±‴ SEM). Using the factor $\mu_{\mathrm{map}} = 2$ to take into account that *in-vitro* estimates were used, we obtain the final estimate of $\gamma = 7.55 \pm 3.94$ (mean±SEM).

Rate constant of CE transfer from HDL to VLDL ($k_{\mathrm{HV}}^{\mathrm{CETP}}$). In [20], the unidirectional movement of CE from HDL to VLDL was quantified using a two -pool model for CE in the Apo B-100 particle classes (VLDL and LDL) and a single pool for CE in HDL particles. Using the data from $n = 3$ subjects, $k_{\mathrm{HV}}^{\mathrm{CETP}}$ is estimated to be 2.24 ± 1.31 pool/day (mean±SD). The rate of CE movement from HDL particles to VLDL has also been quantified in [21]. In this compartmental analysis, a 3-pool model has been used for CE in Apo-B particles (VLDL, IDL and LDL) and bidirectionality of transfer has been assumed between HDL and VLDL as well as between HDL and LDL. Due to the fact that our model does not account for IDL, the CE transfers for this density class are pooled into those of VLDL. For $n = 7$ normal subjects, the net transfers of CE from HDL to VLDL and IDL are 36.5 ± 9.5 mg/dL/day. Normalizing by the individual concentrations of HDL-CE, this gives the estimate of $k_{\mathrm{HV}}^{\mathrm{CETP}} = 1.14 \pm 0.37$ pool/day (mean±SD). By pooling the data sets from both Ouguerram *et al* [20] and Schwartz *et al* [21] and using $\mu_{\mathrm{map}} = 2$ to account for the difference in the structures of compartmental models, we obtain: $k_{\mathrm{HV}}^{\mathrm{CETP}} = 1.47 \pm 0.58$ pool/day (mean±SEM).

Rate constant of CE transfer from HDL to LDL ($k_{\mathrm{HL}}^{\mathrm{CETP}}$). In [20], the movement of CE from HDL to LDL was quantified using a two -pool model for CE in the Apo B-100 particle classes (VLDL and LDL) and a single pool for CE in HDL particles. Using the data from the 3 subjects, $k_{\mathrm{HL}}^{\mathrm{CETP}}$ is estimated to be 9.20 ± 2.54 pool/day (mean±SD). A different estimate is obtained using the data for $n = 7$ normal subjects given in [21]: by dividing the rates of CE movement from HDL particles to LDL by the concentrations of HDL-CE at the individual level, $k_{\mathrm{HL}}^{\mathrm{CETP}}$ is estimated to be 3.88 ± 2.11 pool/day (mean±SD). By pooling the data sets from both Ouguerram *et al* [20] and Schwartz *et al* [21] and using $\mu_{\mathrm{map}} = 2$ to account for the difference in the structures of compartmental models, we obtain: $k_{\mathrm{HL}}^{\mathrm{CETP}} = 5.47 \pm 2.05$ pool/day (mean±SEM).

Rate constant of CE transfer from LDL to HDL ($k_{\mathrm{LH}}^{\mathrm{CETP}}$). In [20], the rate of CE transfer from LDL to HDL was quantified using a two -pool model for CE in the Apo B-100 particle classes (VLDL and LDL) and a single pool for CE in HDL particles. Using the data from the 3 subjects, $k_{\mathrm{LH}}^{\mathrm{CETP}}$ is estimated to be 3.12 ± 1.17 pool/day (mean±SD). An alternative estimate is obtained using the data for $n = 7$ normal subjects given in [21]: by dividing the rates of CE movement from LDL particles to HDL by the concentrations of LDL-CE at the individual level, $k_{\mathrm{LH}}^{\mathrm{CETP}}$ is estimated to be 1.49 ± 0.64 pool/day (mean±SD). By pooling the data sets from both Ouguerram *et al* [20] and Schwartz *et al* [21] and using $\mu_{\mathrm{map}} = 2$ to account for the difference in the structures of compartmental models, we obtain: $k_{\mathrm{LH}}^{\mathrm{CETP}} = 1.98 \pm 0.70$ pool/day (mean±SEM).

Rate constant of transfer of CE from VLDL to LDL (k_{VL}). In [20], the rate constant of CE transfer from VLDL to LDL (due primarily to lipolysis) was inferred in $n = 3$ normal subjects: this gives rise to the parameter estimate $k_{\mathrm{VL}} = 7.52 \pm 0.94$ pool/day (mean±SEM).

Flux of CE to VLDL ($r_{\mathrm{in}}^{\mathrm{VLDL}}$). In [20], the flux of CE into the VLDL pool was inferred in $n = 3$ normal subjects to be 0.96 ± 0.8 mg/dL/day (mean±SD). The cholesteryl ester production to VLDL was also measured by Schwartz *et al* in [21], but due to the large uncertainty as represented by the greater than 100% SD in some of the individual data, these values have not been used. Thus, we take $r_{\mathrm{in}}^{\mathrm{VLDL}} = 0.96 \pm 0.46$ mg/dL/day (mean±SEM).

Rate constant of CE elimination from VLDL ($k_{\mathrm{out}}^{\mathrm{VLDL}}$). In [20], the rate constant of CE elimination from the VLDL pool was inferred in $n = 3$ normal subjects to be 0.88 ± 0.64 pool/day (mean±SD). The quantification of CE elimination rate from VLDL was also carried out by Schwartz *et al* in [21], but the mean of the data was not shown in the paper because most values were undefined (fractional SD >80%). Thus, we use only the values given by Ouguerram *et al* [20] and take $k_{\mathrm{out}}^{\mathrm{VLDL}} = 0.88 \pm 0.37$ pool/day (mean±SEM).

Rate constant of CE elimination from LDL ($k_{\mathrm{out}}^{\mathrm{LDL}}$). In [20], the rate constant of CE elimination from the LDL pool was inferred in $n = 3$ normal subjects to be 0.67 ± 0.14 pool/day (mean±SD). The quantification of CE elimination rate from LDL was also carried out by Schwartz *et al* in [21], but the mean of the flux to the extra-hepatic pool was not shown in the paper because most values were undefined (fractional SD >80%). Thus, we use only the value given by Ouguerram *et al* [20] and take $k_{\mathrm{out}}^{\mathrm{LDL}} = 0.67 \pm 0.08$ pool/day (mean±SEM).

Rate constant of SRB1-mediated CE elimination from HDL ($k_{\mathrm{SRB1}}^{\mathrm{HDL}}$). In [20], the rate constant of selective CE elimination from the HDL pool was inferred in $n = 3$ normal subjects to be 0.31 ± 0.20 pool/day (mean±SD). The selective

Table 6. Calibration data: HDL-C and ApoA-I in normal and CETP deficient subjects.

Type	Data	Inazu [81] (mean±SD)	Yamashita [82] (mean±SD)	Asztalos [83] (mean±SD)	Pooled (mean±SEM)
Normal Subjects	*n*	16	20	50	86
	HDL-C	52.9±13.9	50±8	52±14	52±1
	ApoA-I	124±21	140.9±16.1	144±29	139±4
Heterozygotes of CETP deficiency	*n*	20	15	5	40
	HDL-C	66±15	84±25	85±26	75±4
	ApoA-I	149±43	155.3±22.1	154±25	152±5
Homozygotes of CETP deficiency	*n*	10	4	9	23
	HDL-C	163.7±39	193±28	157±29	166±7
	ApoA-I	213±47	233.5±22.3	252±25	232±8

All concentrations are given in mg/dL.
doi:10.1371/journal.pcbi.1003509.t006

uptake of HDL-CE by the liver was not observed in Schwartz *et al* in [21]. Hence, we use only the value given by Ouguerram *et al* [20] and take $k_{\mathrm{SRB1}}^{\mathrm{HDL}} = 0.31 \pm 0.12$ pool/day $(\mathrm{mean} \pm \mathrm{SEM})$.

Rate constant of size-independent holo-particle uptake for α-HDL (k_{holo}^{c}). The FCR of ApoA-I in the α-HDL pool has been estimated to be 0.112 ± 0.026 pool/day (mean±SD, n = 6) using HDL subclasses separated with size exclusion chromatography [22]. In another reference [72], using a separation technique based on agarose gel electrophoresis, the FCR of ApoA-I in the α-HDL pool has been estimated to be 0.17 ± 0.039 pool/day (mean±SD, $n = 6$). Thus, by pooling the data we obtain $k_{\mathrm{holo}}^{c} = 0.14 \pm 0.013$ pool/day (mean±SEM). Finally, using the factor $\mu_{\mathrm{map}} = 2$, we get $k_{\mathrm{holo}}^{c} = 0.14 \pm 0.026$ pool/day (mean±SEM).

Calibration data

In this section, we give the quantitative values and references for the data used in the calibration procedure.

CETP mutation. Lipoprotein data for CETP mutation patients were taken from 3 sources: Inazu *et al* [81], Yamashita *et al* [82] and Asztalos *et al* [83] and were pooled to yield the mean and SEM. In particular, both HDL-C and ApoA-I were available for each of the 3 data sources shown in Table 6. The values for LDL-CE and VLDL-CE for the control subjects were not given in the references for CETP mutation [81–83]; hence, the values from Ouguerram *et al* [20] and Schwartz *et al* [21] were used in Table 7. The value of LDL-CE for CETP heterozygotes was also used for calibrating the model, which was estimated using the given value of LDL-C with an assumption on the ratio of FC/CE for LDL particles. In Asztalos *et al* [83], the ratio of FC/CE for all lipoprotein particle classes of CETP heterozygotes was given as 0.37, which gives CE = 0.73×TC. Given the approximations made, we assumed that LDL-CE = LDL-C $\times (0.7 \pm 0.05)$. There is literature data for LDL-CE and/or VLDL-CE in CETP homozygotes [39–41], but these were not used in the calibration process due to the known inconsistency of the model in lacking the β-LCAT activity [42].

Table 7. Calibration data: CE in ApoB particles.

Type	Data [20,21]	Pooled (mean±SEM)
Normal subjects	*n*	10
	LDL-CE	83±3 mg/dL
	VLDL-CE	5±1 mg/dL
Heterozygotes of CETP deficiency	*n*	23
	LDL-CE (LDL-C ×0.7)	72±9 mg/dL

doi:10.1371/journal.pcbi.1003509.t007

Cholesteryl ester flux. There are 2 literature data sources on the *in-vivo* flux of CE between HDL and ApoB-containing particles: Ouguerram *et al* [20] and Schwartz *et al* [21]. While both data sets have been used in estimating the prior distribution of parameters involved in the exchanges of CE (see Methods section), for the purpose of model calibration a choice between the 2 disparate data needed to be made. Given that the model structure in the description of CE exchanges between HDL, LDL and VLDL is based on that of Ouguerram *et al* [20], it was decided that the same calibration data should be taken for the CE fluxes. The values used are shown in Table 8.

Fractional catabolic rate of apoA-I. Brinton *et al* have shown that a strong association exists between the fractional catabolic rate (FCR) of ApoA-I and the estimated HDL size, using a surrogate marker [43] (Brinton *et al* used HDL-C/(ApoA-I+ApoA-II), we re-analyzed their data taking HDL-C/ApoA-I as the surrogate marker). Their work has demonstrated that as much as 70% of the variability in the FCR of ApoA-I may be attributed to variations in HDL size, as estimated using $\frac{\mathrm{HDL}-\mathrm{C}}{\mathrm{ApoA}-\mathrm{I}}$ [43]. This finding is corroborated with the individual data of ApoA-I metabolism from Schaefer *et al* [44] measured in healthy volunteers. Finally, FCR of ApoA-I was also studied by Ikewaki *et al* [45] in comparing CETP mutation subjects with controls. All

Table 8. Calibration data: CE fluxes.

CE flux (mean±SEM)	Data (mg/dL/day)
HDL to VLDL	64±2
HDL to LDL	268±51
LDL to HDL	266±52

doi:10.1371/journal.pcbi.1003509.t008

these data consistently show that the ApoA-I FCR exhibits an inverse relationship with the surrogate measure of HDL size. However, the trend does not continue indefinitely: even for CETP homozygous subjects with very large particles, ApoA-I FCR appears to reach a minimum of 0.135 pool/day. Hence, we have tried to describe the data in the simplest way, assuming a linear relationship between ApoA-I FCR and $\frac{\mathrm{HDL}-\mathrm{C}}{\mathrm{ApoA}-\mathrm{I}}$, with a lower bound of 0.135. Using this linear assumption, the fit and confidence interval was computed and shown in Figure 4. The piecewise linear fit to the combined data is given by $\mathrm{FCR}_{\mathrm{ApoA}-\mathrm{I}} = \max(0.50 - 0.63 \times \left(\frac{\mathrm{HDL}-\mathrm{C}}{\mathrm{ApoA}-\mathrm{I}}\right), 0.135)$; the mean confidence interval corresponding to 1 SD in the line fit is approximately ± 0.065 pool/day.

Model calibration

In this work, we assume that both the parameter prior and the data error are normally distributed. We employ the methodology of *maximum a posteriori* (MAP) [31] to combine the prior information with calibration data. Due to the conjugacy property [31] of the distributions, the posterior also has a normal distribution and the MAP solution is obtained by solving a nonlinear least squares problem. In our model, most of the parameters have an informative prior. For the set of parameters for which an informative prior is available, let k_{prior} denote the expected value of the prior distribution; otherwise, set $k_{prior} = 0$ to represent the lack of information. We take the covariance matrix for the prior distribution C_k to have a diagonal structure: for parameters k_i that have an informative prior, $(C_k)_{ii}$ is the variance of the prior distribution; for parameters that have an uninformative prior, $(C_k)_{ii} = \infty$. That is, the prior distribution is assumed to be of the form [33]:

$$p(k) \propto \exp\left(-\frac{1}{2}(k - k_{prior})^T C_k^{-1} (k - k_{prior}) \right). \quad (16)$$

Let $d \in \mathbb{R}^m$ denote the vector of calibration data and $G(k)$ the nonlinear mapping from model parameters to the observation, representing the model simulation of the data. Let C_d denote the covariance matrix for the data. Hence, the conditional distribution of the data given the model parameter k is [33]:

$$f(d|k) \propto \exp\left(-\frac{1}{2}(G(k) - d)^T C_d^{-1} (G(k) - d) \right). \quad (17)$$

Thus, the posterior distribution $q(k|d)$ for the model parameters is given by

$$q(k|d) \propto f(d|k)p(k) = \exp\left(-\frac{1}{2}(G(k) - d)^T C_d^{-1} (G(k) - d) - \frac{1}{2}(k - k_{prior})^T C_k^{-1} (k - k_{prior}) \right). \quad (18)$$

To find the MAP solution, the following nonlinear least squares problem is solved: with the objective function defined as,

$$\chi^2(k) \equiv (G(k) - d)^T C_d^{-1} (G(k) - d) + (k - k_{prior})^T C_k^{-1} (k - k_{prior}), \quad (19)$$

the MAP solution is the minimizer:

$$k_{MAP} \leftarrow \min_k \chi^2(k). \quad (20)$$

Using parameter priors as given in Table 5 and calibration data as described in the previous section, the nonlinear least-squares problem was solved using genetic algorithm ga from the Matlab® Global Optimization Toolbox of MathWorks (http://www.mathworks.com/) to obtain k_{MAP}. In particular, the hybrid option was selected: 100 generations of the genetic algorithm was run with a PopulationSize = 500, followed by constrained minimization (fmincon) using the setting MaxFunEvals = 10000, MaxIter = 1000. In all numerical integration of ODEs, the relative and absolute tolerances were set to 10^{-9}.

Estimation of 95% confidence intervals

The confidence interval is estimated using the following procedure: parameters are sampled around k_{MAP} and for each parameter the $\Delta\chi^2$ (with respect to its minimum, $\chi^2(k_{\mathrm{MAP}})$) is computed according to the expression (19). An estimate of the confidence region is obtained by examining the set of all parameters that lie within $\Delta\chi^2 \leq \delta$, where δ is computed from the number of degrees of freedom (df) and the desired confidence level [84]. Using df = 29 for the model and choosing the 95% confidence level, $\delta = 42.557$. A set of 1000 parameters satisfying $\Delta\chi^2 \leq 42.557$ are selected in estimating confidence intervals shown in the paper.

Simulation of tracer kinetic studies

The model simulations of the tracer kinetic experiment with labelled ApoA-I and the calculation of the FCR of ApoA-I were carried out using the technique of complex variable differentiation [85]. In particular, a small quantity of imaginary number representing the radio-labelled dose of ApoA-I is added to the lipid-poor pool at the start of tracer experiment and the imaginary component of the numerical solution is extracted to represent the dose remaining in the two pools of ApoA-I (lipid-poor and α-HDL). This method relies on the complex extension of analytic functions from the real line, which can be easily implemented on the Matlab platform [85]. As compared to the finite-differencing approach, the complex variable methodology does not suffer from subtractive cancellation error and hence is more accurate [85]. While this approach has not been applied to tracer kinetic simulations, it has been applied to the sensitivity analysis of biological models [86,87].

Supporting Information

File S1 LMK model implementation in SimBiology and Matlab formats.
(ZIP)

Acknowledgments

We would like to thank Daniel Serafin for his contribution in digitizing ApoA-I tracer kinetics data from Figure 3 of Ikewaki *et al*, JLR 1993 and acknowledge anonymous reviewers whose detailed critique of the original manuscript helped to strengthen the final version. This paper is dedicated to the memory of Philippe Vuilleumier, a long time member of the MIT Club of Switzerland.

Author Contributions

Analyzed the data: JL NAM. Contributed reagents/materials/analysis tools: JL NAM. Wrote the paper: JL KH MNN EAB NAM.

References

1. Di Angelantonio E, Sarwar N, Perry P, Kaptoge S, Ray KK, et al. (2009) Major lipids, apolipoproteins, and risk of vascular disease. JAMA 302: 1993–2000.
2. Larach DB, deGoma EM, Rader DJ (2012) Targeting high density lipoproteins in the prevention of cardiovascular disease? Curr Cardiol Rep 14: 684–691.
3. Hersberger M, von Eckardstein A (2005) Modulation of high-density lipoprotein cholesterol metabolism and reverse cholesterol transport. Handb Exp Pharmacol 170: 537–561.
4. Rothblat GH, Phillips MC (2010) High-density lipoprotein heterogeneity and function in reverse cholesterol transport. Curr Opin Lipidol 21: 229–238.
5. Barter PJ, Caulfield M, Eriksson M, Grundy SM, Kastelein JJ, et al. (2007) Effects of torcetrapib in patients at high risk for coronary events. N Engl J Med 357: 2109–2122.
6. Boden WE, Probstfield JL, Anderson T, Chaitman BR, Desvignes-Nickens P, et al. (2011) Niacin in patients with low HDL cholesterol levels receiving intensive statin therapy. N Engl J Med 365: 2255–2267.
7. Schwartz GG, Olsson AG, Abt M, Ballantyne CM, Barter PJ, et al. (2012) Effects of dalcetrapib in patients with a recent acute coronary syndrome. N Engl J Med 367: 2089–2099.
8. Rosenson RS, Brewer HB, Davidson WS, Fayad ZA, Fuster V, et al. (2012) Cholesterol efflux and atheroprotection: advancing the concept of reverse cholesterol transport. Circulation 125: 1905–1919.
9. Rader DJ, Tall AR (2012) The not-so-simple HDL story: Is it time to revise the HDL cholesterol hypothesis? Nat Med 18: 1344–1346.
10. Heinecke JW (2012) The not-so-simple HDL story: A new era for quantifying HDL and cardiovascular risk? Nat Med 18: 1346–1347.
11. de Graaf AA, van Schalkwijk DB (2011) Computational models for analyzing lipoprotein profiles. Clinical Lipidology 6: 25–33.
12. Lu J, Mazer NA, Hübner K (2013) Mathematical models of lipoprotein metabolism and kinetics -current status and future perspectives. Clinical Lipidology 8: 595–604.
13. Potter LK, Sprecher DL, Walker MC, Tobin FL (2009) Mechanism of inhibition defines CETP activity: a mathematical model for CETP in vitro. J Lipid Res 50: 2222–2234.
14. van Schalkwijk DB, de Graaf AA, van Ommen B, van Bochove K, Rensen PC, et al. (2009) Improved cholesterol phenotype analysis by a model relating lipoprotein life cycle processes to particle size. J Lipid Res 50: 2398–2411.
15. Knoblauch H, Schuster H, Luft FC, Reich J (2000) A pathway model of lipid metabolism to predict the effect of genetic variability on lipid levels. J Mol Med 78: 507–515.
16. Hübner K, Schwager T, Winkler K, Reich JG, Holzhütter HG (2008) Computational lipidology: predicting lipoprotein density profiles in human blood plasma. PLoS Comput Biol 4: e1000079.
17. van de Pas NC, Woutersen RA, van Ommen B, Rietjens IM, de Graaf AA (2012) A physiologically based in silico kinetic model predicting plasma cholesterol concentrations in humans. J Lipid Res 53: 2734–2746.
18. Mc Auley MT, Wilkinson DJ, Jones JJ, Kirkwood TB (2012) A whole-body mathematical model of cholesterol metabolism and its age-associated dysregulation. BMC Syst Biol 6: 130.
19. Tiemann CA, Vanlier J, Oosterveer MH, Groen AK, Hilbers PA, et al. (2013) Parameter trajectory analysis to identify treatment effects of pharmacological interventions. PLoS Comput Biol 9: e1003166.
20. Ouguerram K, Krempf M, Maugeais C, Maugere P, Darmaun D, et al. (2002) A new labeling approach using stable isotopes to study in vivo plasma cholesterol metabolism in humans. Metab Clin Exp 51: 5–11.
21. Schwartz CC, VandenBroek JM, Cooper PS (2004) Lipoprotein cholesteryl ester production, transfer, and output in vivo in humans. J Lipid Res 45: 1594–1607.
22. Chetiveaux M, Ouguerram K, Zair Y, Maugere P, Falconi I, et al. (2004) New model for kinetic studies of HDL metabolism in humans. Eur J Clin Invest 34: 262–267.
23. Rye KA, Clay MA, Barter PJ (1999) Remodelling of high density lipoproteins by plasma factors. Atherosclerosis 145: 227–238.
24. Adiels M, Packard C, Caslake MJ, Stewart P, Soro A, et al. (2005) A new combined multicompartmental model for apolipoprotein B-100 and triglyceride metabolism in VLDL subfractions. J Lipid Res 46: 58–67.
25. Mazer NA, Giulianini F, Paynter NP, Jordan P, Mora S (2013) A comparison of the theoretical relationship between HDL size and the ratio of HDL cholesterol to apolipoprotein A-I with experimental results from the Women's Health Study. Clin Chem 59: 949–958.
26. Scanu AM, Edelstein C (2008) HDL: bridging past and present with a look at the future. FASEB J 22: 4044–4054.
27. Kontush A, Chapman MJ (2006) Functionally defective high-density lipoprotein: a new therapeutic target at the crossroads of dyslipidemia, inammation, and atherosclerosis. Pharmacol Rev 58: 342–374.
28. Moestrup SK, Kozyraki R (2000) Cubilin, a high-density lipoprotein receptor. Curr Opin Lipidol 11: 133–140.
29. Martinez LO, Jacquet S, Esteve JP, Rolland C, Cabezon E, et al. (2003) Ectopic beta-chain of ATP synthase is an apolipoprotein A-I receptor in hepatic HDL endocytosis. Nature 421: 75–79.
30. Chapman MJ, Le Goff W, Guerin M, Kontush A (2010) Cholesteryl ester transfer protein: at the heart of the action of lipid-modulating therapy with statins, fibrates, niacin, and cholesteryl ester transfer protein inhibitors. Eur Heart J 31: 149–164.
31. Aster R, Borchers B, Thurber C (2005) Parameter Estimation and Inverse Problems. Academic Press.
32. Klinke DJ (2009) An empirical Bayesian approach for model-based inference of cellular signaling networks. BMC Bioinformatics 10: 371.
33. Eydgahi H, Chen WW, Muhlich JL, Vitkup D, Tsitsiklis JN, et al. (2013) Properties of cell death models calibrated and compared using Bayesian approaches. Mol Syst Biol 9: 644.
34. Gisleskog PO, Karlsson MO, Beal SL (2002) Use of prior information to stabilize a population data analysis. J Pharmacokinet Pharmacodyn 29: 473–505.
35. Jonsson F, Jonsson EN, Bois FY, Marshall S (2007) The application of a Bayesian approach to the analysis of a complex, mechanistically based model. J Biopharm Stat 17: 65–92.
36. Vergeer M, Korporaal SJ, Franssen R, Meurs I, Out R, et al. (2011) Genetic variant of the scavenger receptor BI in humans. N Engl J Med 364: 136–145.
37. Vaziri ND, Navab M, Fogelman AM (2010) HDL metabolism and activity in chronic kidney disease. Nat Rev Nephrol 6: 287–296.
38. Fabre AC, Vantourout P, Champagne E, Terce F, Rolland C, et al. (2006) Cell surface adenylate kinase activity regulates the F(1)-ATPase/P2Y (13)-mediated HDL endocytosis pathway on human hepatocytes. Cell Mol Life Sci 63: 2829–2837.
39. Ritsch A, Drexel H, Amann FW, Pfeifhofer C, Patsch JR (1997) Deficiency of cholesteryl ester transfer protein. Description of the molecular defect and the dissociation of cholesteryl ester and triglyceride transport in plasma. Arterioscler Thromb Vasc Biol 17: 3433–3441.
40. Ikewaki K, Nishiwaki M, Sakamoto T, Ishikawa T, Fairwell T, et al. (1995) Increased catabolic rate of low density lipoproteins in humans with cholesteryl ester transfer protein deficiency. J Clin Invest 96: 1573–1581.
41. Teh EM, Dolphin PJ, Breckenridge WC, Tan MH (1998) Human plasma CETP deficiency: identification of a novel mutation in exon 9 of the CETP gene in a Caucasian subject from North America. J Lipid Res 39: 442–456.
42. Carlson LA, Holmquist L (1985) Evidence for the presence in human plasma of lecithin: cholesterol acyltransferase activity (beta-LCAT) specifically esterifying free cholesterol of combined pre-betaand beta-lipoproteins. Studies of fish eye disease patients and control subjects. Acta Med Scand 218: 197–205.
43. Brinton EA, Eisenberg S, Breslow JL (1994) Human HDL cholesterol levels are determined by apoA-I fractional catabolic rate, which correlates inversely with estimates of HDL particle size. Effects of gender, hepatic and lipoprotein lipases, triglyceride and insulin levels, and body fat distribution. Arterioscler Thromb 14: 707–720.
44. Schaefer EJ, Zech LA, Jenkins LL, Bronzert TJ, Rubalcaba EA, et al. (1982) Human apolipoprotein A-I and A-II metabolism. J Lipid Res 23: 850–862.
45. Ikewaki K, Rader DJ, Sakamoto T, Nishiwaki M, Wakimoto N, et al. (1993) Delayed catabolism of high density lipoprotein apolipoproteins A-I and A-II in human cholesteryl ester transfer protein deficiency. J Clin Invest 92: 1650–1658.
46. Asztalos BF, Brousseau ME, McNamara JR, Horvath KV, Roheim PS, et al. (2001) Subpopulations of high density lipoproteins in homozygous and heterozygous Tangier disease. Atherosclerosis 156: 217–225.
47. Santos RD, Schaefer EJ, Asztalos BF, Polisecki E, Wang J, et al. (2008) Characterization of high density lipoprotein particles in familial apolipoprotein A-I deficiency. J Lipid Res 49: 349–357.
48. Ikewaki K, Rader DJ, Schaefer JR, Fairwell T, Zech LA, et al. (1993) Evaluation of apoA-I kinetics in humans using simultaneous endogenous stable isotope and exogenous radiotracer methods. J Lipid Res 34: 2207–2215.
49. Moss R, Grosse T, Marchant I, Lassau N, Guey_er F, et al. (2012) Virtual patients and sensitivity analysis of the Guyton model of blood pressure regulation: towards individualized models of wholebody physiology. PLoS Comput Biol 8: e1002571.
50. Schwartz GG, Olsson AG, Barter PJ (2013) Dalcetrapib in patients with an acute coronary syndrome. N Engl J Med 368: 869–870.
51. Clark RW, Sutfin TA, Ruggeri RB, Willauer AT, Sugarman ED, et al. (2004) Raising high-density lipoprotein in humans through inhibition of cholesteryl ester transfer protein: an initial multidose study of torcetrapib. Arterioscler Thromb Vasc Biol 24: 490–497.
52. Cannon CP, Shah S, Dansky HM, Davidson M, Brinton EA, et al. (2010) Safety of anacetrapib in patients with or at high risk for coronary heart disease. N Engl J Med 363: 2406–2415.
53. Voight BF, Peloso GM, Orho-Melander M, Frikke-Schmidt R, Barbalic M, et al. (2012) Plasma HDL cholesterol and risk of myocardial infarction: a mendelian randomisation study. Lancet 380: 572–580.
54. Mackey RH, Greenland P, Goff DC, Lloyd-Jones D, Sibley CT, et al. (2012) High-density lipoprotein cholesterol and particle concentrations, carotid atherosclerosis, and coronary events: MESA (multi-ethnic study of atherosclerosis). J Am Coll Cardiol 60: 508–516.
55. Sethi AA, Sampson M, Warnick R, Muniz N, Vaisman B, et al. (2010) High pre-beta1 HDL concentrations and low lecithin: cholesterol acyltransferase activities

are strong positive risk markers for ischemic heart disease and independent of HDL-cholesterol. Clin Chem 56: 1128–1137.
56. Kane JP, Malloy MJ (2012) Prebeta-1 HDL and coronary heart disease. Curr Opin Lipidol 23: 367–371.
57. Kaess BM, Tomaszewski M, Braund PS, Stark K, Rafelt S, et al. (2011) Large-scale candidate gene analysis of HDL particle features. PLoS ONE 6: e14529.
58. Rothblat GH, de la Llera-Moya M, Atger V, Kellner-Weibel G, Williams DL, et al. (1999) Cell cholesterol efflux: integration of old and new observations provides new insights. J Lipid Res 40: 781–796.
59. Patel DC, Albrecht C, Pavitt D, Paul V, Pourreyron C, et al. (2011) Type 2 diabetes is associated with reduced ATP-binding cassette transporter A1 gene expression, protein and function. PLoS ONE 6: e22142.
60. Paul V, Meyer HH, Leidl K, Soumian S, Albrecht C (2008) A novel enzyme immunoassay specific for ABCA1 protein quantification in human tissues and cells. J Lipid Res 49: 2259–2267.
61. Nanjee MN, Brinton EA (2000) Very small apolipoprotein A-I-containing particles from human plasma: isolation and quantification by high-performance size-exclusion chromatography. Clin Chem 46: 207–223.
62. Asztalos BF, Collins D, Cupples LA, Demissie S, Horvath KV, et al. (2005) Value of high-density lipoprotein (HDL) subpopulations in predicting recurrent cardiovascular events in the Veterans Affairs HDL Intervention Trial. Arterioscler Thromb Vasc Biol 25: 2185–2191.
63. Asztalos BF, Batista M, Horvath KV, Cox CE, Dallal GE, et al. (2003) Change in alpha1 HDL concentration predicts progression in coronary artery stenosis. Arterioscler Thromb Vasc Biol 23: 847–852.
64. Hirayama S, Miida T, Miyazaki O, Aizawa Y (2007) Pre beta1-HDL concentration is a predictor of carotid atherosclerosis in type 2 diabetic patients. Diabetes Care 30: 1289–1291.
65. de Vries R, Perton FG, van Tol A, Dullaart RP (2012) Carotid intima media thickness is related positively to plasma pre -high density lipoproteins in non-diabetic subjects. Clin Chim Acta 413: 473–477.
66. Guey LT, Pullinger CR, Ishida BY, O'Connor PM, Zellner C, et al. (2011) Relation of increased prebeta-1 high-density lipoprotein levels to risk of coronary heart disease. Am J Cardiol 108: 360–366.
67. Shah A, Rader DJ, Millar JS (2010) The effect of PPAR-alpha agonism on apolipoprotein metabolism in humans. Atherosclerosis 210: 35–40.
68. Apostoli AJ, Nicol CJ (2012) PPAR Medicines and Human Disease: The ABCs of It All. PPAR Res 2012: 504918.
69. Rodrigueza WV, Williams KJ, Rothblat GH, Phillips MC (1997) Remodeling and shuttling. Mechanisms for the synergistic effects between different acceptor particles in the mobilization of cellular cholesterol. Arterioscler Thromb Vasc Biol 17: 383–393.
70. Tchoua U, Gillard BK, Pownall HJ (2010) HDL superphospholipidation enhances key steps in reverse cholesterol transport. Atherosclerosis 209: 430–435.
71. Shen BW, Scanu AM, Kezdy FJ (1977) Structure of human serum lipoproteins inferred from compositional analysis. Proc Natl Acad Sci USA 74: 837–841.
72. Li X, Stolinski M, Umpleby AM (2012) Development of a method to measure pre–β HDL and α–HDL apoA-I enrichment for stable isotopic studies of HDL kinetics. Lipids 47: 1011–1018.
73. Braschi S, Neville TA, Maugeais C, Ramsamy TA, Seymour R, et al. (2000) Role of the kidney in regulating the metabolism of HDL in rabbits: evidence that iodination alters the catabolism of apolipoprotein A-I by the kidney. Biochemistry 39: 5441–5449.
74. Bojanovski D, Gregg RE, Zech LA, Meng MS, Bishop C, et al. (1987) In vivo metabolism of proapolipoprotein A-I in Tangier disease. J Clin Invest 80: 1742–1747.
75. Schaefer EJ, Anderson DW, Zech LA, Lindgren FT, Bronzert TB, et al. (1981) Metabolism of high density lipoprotein subfractions and constituents in Tangier disease following the infusion of high density lipoproteins. J Lipid Res 22: 217–228.
76. Cavigiolio G, Geier EG, Shao B, Heinecke JW, Oda MN (2010) Exchange of apolipoprotein A-I between lipid-associated and lipid-free states: a potential target for oxidative generation of dysfunctional high density lipoproteins. J Biol Chem 285: 18847–18857.
77. Cheung MC, Wolf AC, Knopp RH, Foster DM (1992) Protein transfer between A-I-containing lipoprotein subpopulations: evidence of non-transferable A-I in particles with A-II. Biochim Biophys Acta 1165: 68–77.
78. Lund-Katz S, Nguyen D, Dhanasekaran P, Kono M, Nickel M, et al. (2010) Surface plasmon resonance analysis of the mechanism of binding of apoA-I to high density lipoprotein particles. J Lipid Res 51: 606–617.
79. Castro GR, Fielding CJ (1988) Early incorporation of cell-derived cholesterol into pre-betamigrating high-density lipoprotein. Biochemistry 27: 25–29.
80. Sorci-Thomas MG, Owen JS, Fulp B, Bhat S, Zhu X, et al. (2012) Nascent high density lipoproteins formed by ABCA1 resemble lipid rafts and are structurally organized by three apoA-I monomers. J Lipid Res 53: 1890–1909.
81. Inazu A, Brown ML, Hesler CB, Agellon LB, Koizumi J, et al. (1990) Increased high-density lipoprotein levels caused by a common cholesteryl-ester transfer protein gene mutation. N Engl J Med 323: 1234–1238.
82. Yamashita S, Hui DY, Wetterau JR, Sprecher DL, Harmony JA, et al. (1991) Characterization of plasma lipoproteins in patients heterozygous for human plasma cholesteryl ester transfer protein (CETP) deficiency: plasma CETP regulates high-density lipoprotein concentration and composition. Metab Clin Exp 40: 756–763.
83. Asztalos BF, Horvath KV, Kajinami K, Nartsupha C, Cox CE, et al. (2004) Apolipoprotein composition of HDL in cholesteryl ester transfer protein deficiency. J Lipid Res 45: 448–455.
84. Press WH, Teukolsky SA, Vetterling WT, Flannery BP (1992) Numerical recipes in C (2nd ed.): the art of scientific computing. Cambridge, UK: Cambridge University Press.
85. Martins JRRA, Sturdza P, Alonso JJ (2003) The complex-step derivative approximation. ACM Trans Math Software 29: 245–262.
86. Apgar JF, Witmer DK, White FM, Tidor B (2010) Sloppy models, parameter uncertainty, and the role of experimental design. Mol Biosyst 6: 1890–1900.
87. Wei XN, Han BC, Zhang JX, Liu XH, Tan CY, et al. (2011) An integrated mathematical model of thrombin-, histamine-and VEGF-mediated signalling in endothelial permeability. BMC Syst Biol 5: 112.
88. Velez-Carrasco W, Lichtenstein AH, Li Z, Dolnikowski GG, Lamon-Fava S, et al. (2000) Apolipoprotein A-I and A-II kinetic parameters as assessed by endogenous labeling with [(2)H(3)]leucine in middle-aged and elderly men and women. Arterioscler Thromb Vasc Biol 20: 801–806.
89. Schaefer EJ, Santos RD, Asztalos BF (2010) Marked HDL deficiency and premature coronary heart disease. Curr Opin Lipidol 21: 289–297.
90. Barter PJ (2002) Hugh Sinclair Lecture: the regulation and remodelling of HDL by plasma factors. Atheroscler Suppl 3: 39–47.
91. Miyazaki O, Fukamachi I, Mori A, Hashimoto H, Kawashiri MA, et al. (2009) Formation of prebeta1-HDL during lipolysis of triglyceride-rich lipoprotein. Biochem Biophys Res Commun 379: 55–59.
92. Liang HQ, Rye KA, Barter PJ (1994) Dissociation of lipid-free apolipoprotein A-I from high density lipoproteins. J Lipid Res 35: 1187–1199.
93. Settasatian N, Duong M, Curtiss LK, Ehnholm C, Jauhiainen M, et al. (2001) The mechanism of the remodeling of high density lipoproteins by phospholipid transfer protein. J Biol Chem 276: 26898–26905.